Journal of Medicinal Chemistry

pubs.acs.org/jmc

Article

Discovery and Characterization of a Bicyclic Peptide (Bicycle) Binder to Thymic Stromal Lymphopoietin

Frank Narjes,* Fredrik Edfeldt, Jens Petersen, Linda Öster, Corinne Hamblet, James Bird, Peter Bold, Rebecca Rae, Elisabeth Bäck, Stina Stomilovic, Pavol Zlatoidsky, Tor Svensson, Lotta Hidestål, Lavaniya Kunalingam, Igor Shamovsky, Leonardo De Maria, Euan Gordon, Richard J. Lewis, Sophie Watcham, Katerine van Rietschoten, Gemma E. Mudd, Helen Harrison, Liuhong Chen, and Michael J. Skynner

Cite This: https://doi.org/10.1021/acs.jmedchem.3c02163

Read Online

ACCESS | Metrics & More | Article Recommendations | Supporting Information

ABSTRACT: Thymic stromal lymphopoietin (TSLP) is an epithelial-derived pro-inflammatory cytokine involved in the development of asthma and other atopic diseases. We used Bicycle Therapeutics' proprietary phage display platform to identify bicyclic peptides (Bicycles) with high affinity for TSLP, a target that is difficult to drug with conventional small molecules due to the extended protein−protein interactions it forms with both receptors. The hit series was shown to bind to TSLP in a hotspot, that is also used by IL-7Rα. Guided by the first X-ray crystal structure of a small peptide binding to TSLP and the identification of key metabolites, we were able to improve the proteolytic stability of this series in lung S9 fractions without sacrificing binding affinity. This resulted in the potent Bicycle **46** with nanomolar affinity to TSLP (K_D = 13 nM), low plasma clearance of 6.4 mL/min/kg, and an effective half-life of 46 min after intravenous dosing to rats.

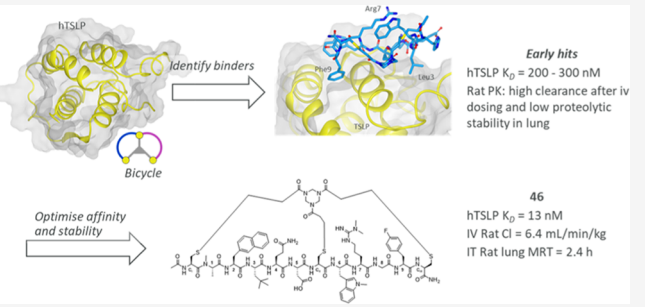

INTRODUCTION

There has been considerable acceleration in drug discovery efforts to identify novel macrocyclic peptide medicines, with multiple approved therapies for a diverse set of indications and a broad pipeline of preclinical and clinical assets.[1−3] These conformationally constrained peptides can target proteins that are hard, or impossible, to drug with conventional Lipinski-compliant small molecules.[4−9] Protein−protein interactions (PPI) usually require a contact area of 1500−3000 Å^2, while small molecules only cover ca. 300−1000 Å^2, due to their low molecular weight. In addition, peptides have found strong utility as targeting moieties, delivering therapeutic payloads such as peptide toxins or oligonucleotides to specific cell types or tissues.[10,11] Here, we were interested in investigating the potential for macrocyclic peptides as an alternative modality to small molecules or antibodies for the treatment of lung diseases. When compared to small molecules, constrained cyclic peptides have the advantage of being able to disrupt PPIs with high potency, and with respect to antibodies, their lower cost of production, more rapid extravasation, and higher tissue penetration present significant advantages.[12]

Despite recent progress, peptide therapeutics still lack significant cell penetration and oral bioavailability, as these properties are highly dependent on size and amino acid composition. To advance our efforts and understanding in this area and avoid these difficulties, we opted to investigate the pharmacology of an extracellular target through delivery via the inhaled route of administration, which is also often the chosen route for the treatment of asthma or chronic obstructive pulmonary disease.[13] We chose to exemplify this through targeting thymic stromal lymphopoietin (TSLP), a cytokine released by epithelial cells in the lung in response to external insults that mediates type 2 immunity. Our aim was to identify bicyclic peptides binding to TSLP using Bicycle Therapeutics' proprietary bicyclic phage display platform, which has previously been shown to be highly effective at identifying ligands to a wide range of biological targets.[11,14−16] Additionally, we wanted to characterize and optimize the pharmacokinetics and the proteolytic stability in plasma and lung of these Bicycles.

TSLP is part of a group of three cytokines, including interleukins IL-25 and IL-33, called alarmins. These are released by epithelial cells in the lung in response to external

Received: November 18, 2023
Revised: December 21, 2023
Accepted: January 15, 2024

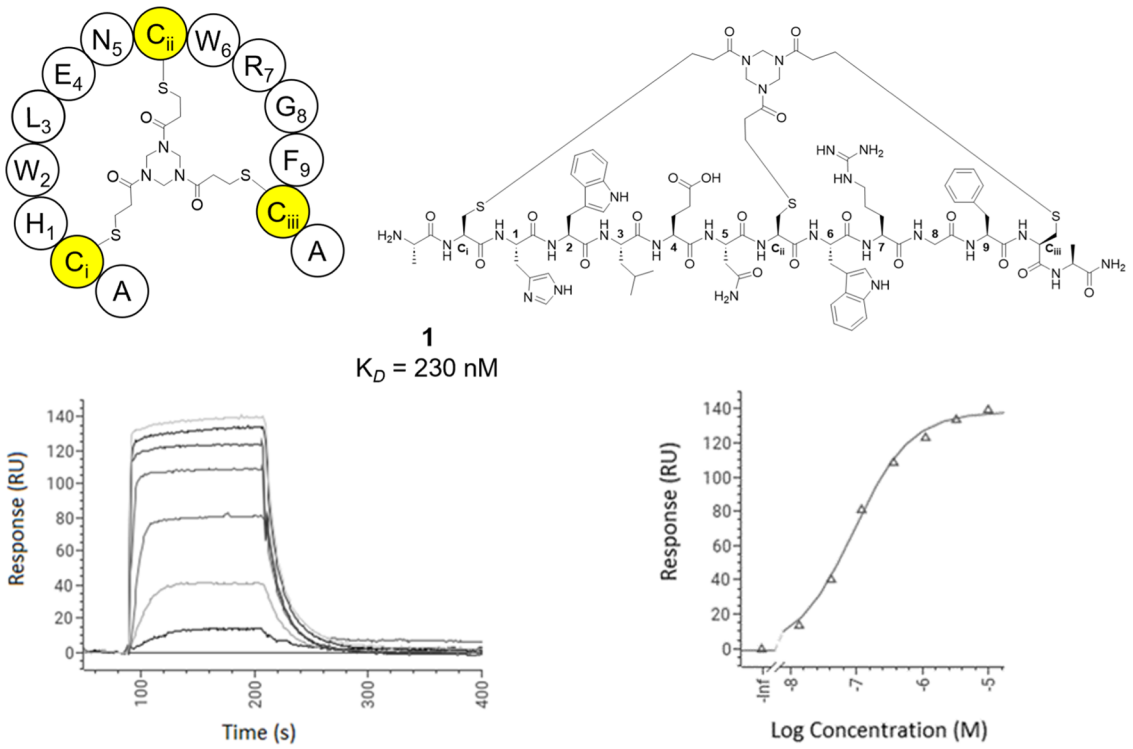

Figure 1. Representation and chemical structure of Bicycle **1**, SPR sensorgrams, and dose−response curve for binding to immobilized hTSLP.

insults and act to mediate type 2 immunity. TSLP exerts its effect by inducing the heterodimerization of its cognate receptor (TSLPR) with the shared IL-7 receptor α-chain (IL-7Rα) on the cell surface, leading to the initiation of a signaling cascade via the JAK-STAT pathway.[17] This induces maturation and survival of dendritic cells, as well as increasing secretion of chemokines, such as CCL17 and CCL22, which attract and maintain IL-4 and IL-5 producing T cells and innate lymphoid cells.[17−19] Its abnormal production is linked to a range of pathologies such as asthma and atopic dermatitis, other immune-mediated diseases, and cancer.[20,21] TSLP seems to play a central role in driving airway inflammation and asthma exacerbations.

Recently published X-ray structures of the mouse and the human TSLP ternary signaling complexes show that the interactions of TSLP with both receptor subunits are governed by extensive PPIs.[22,23] Tezepelumab, a monoclonal antibody that binds to TSLP and prevents binding to its cell surface receptor TSLPR, has shown clinical efficacy in reducing exacerbations and symptoms in asthmatics and was recently approved for the treatment of severe asthma.[24−27] Other biologics targeting TSLP, including the inhaled antibody fragment CSJ117, are currently progressing through advanced clinical trials.[28,29]

A range of approaches have been trailed to target TSLP signaling; these include linear peptides derived from the TSLP−TSLPR interface and small molecules obtained from virtual or fragment screening.[30−32] To date, none of these attempts has identified potent binders or inhibitors. Here, we describe the identification and optimization of a series of Bicycles binding to TSLP. We characterize the binding site and optimize the potency and proteolytic stability of these compounds. The resulting Bicycles bind to TSLP at a site used by the IL-7Rα subunit, have low nanomolar affinity for TSLP, and showed improved stability in rat plasma and rat lung S9 fraction.

RESULTS AND DISCUSSION

Hits from Bicycle Phage Display, Affinity Maturation, and Initial Structure Activity Relationship (SAR). Twenty combinatorial peptide libraries having the format AC(X)$_m$C-(X)$_n$CA, where "m" and "n" varied from a minimum of two to a maximum of nine amino acids and X represents any of the 19 standard proteogenic amino acids (excluding cysteine), were produced on bacteriophage (phage) and cyclized with 1,3,5-triacryloyl-1,3,5-triazinane (TATA) as previously described.[33,34] These phage libraries were panned against commercially sourced recombinant human TSLP that had been preferentially chemically biotinylated on the *N*-terminus to avoid occlusion of the receptor-binding surfaces on the protein. After 4 rounds of panning, phage binders were sequenced, and Bicycles were chemically synthesized to confirm binding.

From these initial phage outputs, several clusters of sequences were identified, including a WXGF motif within a 5 × 4 library (5 randomized residues in the first loop and 4 randomized residues in the second loop).

To expand the chemical space around these Bicycles, bespoke phage libraries were built based on the WXGF cluster where some common residues were maintained, and variant residues were allowed to be fully randomized. This led to the selection of arginine as the optimal residue for X in the second loop. Based on the best sequences obtained from this initial cycle of affinity maturation, additional libraries were subsequently built, to explore whether extending the peptide beyond the cyclized region at the N- and C-termini would confer any additional affinity improvement.

Several of the hits from the phage library were then prepared as C-terminal amides, using standard Fmoc solid-phase

https://doi.org/10.1021/acs.jmedchem.3c02163
J. Med. Chem. XXXX, XXX, XXX−XXX

chemistry to prepare the linear peptide and cyclization with TATA as previously described.[35] Their affinity toward TSLP was assessed using surface plasma resonance (SPR) measurements with TSLP immobilized on a biosensor chip. Binding of several 5 × 4 peptides to TSLP was confirmed, but only compound **1** showed submicromolar affinity and was chosen for further investigation (Figure 1).

The binding affinity of **1** was improved 3-fold by substituting 2 amino acids in loop 1, His at position 1, and Asn at position 5 for Gln and Asp, respectively, resulting in **2** (K_D = 75 nM, Table 1). Extension of **2** on the N- or C-terminus with 3−5 amino acids led at best to a 2.5-fold gain in potency, as exemplified for analogues **3**-**6**, suggesting that the elongated termini did not engage in strong interactions with TSLP. Complete removal of the terminal alanine residues in **1** and **2** and introduction of an N-terminal acetyl group led to compounds **7** and **8**, respectively, which showed only a slight loss in binding affinity. These truncated compounds were subsequently used as lead structures for further investigations. Alongside, we also prepared compound **9**, the enantiomer of **7**, composed entirely of D-amino acids. As expected, it did not show any affinity toward TSLP, when tested by SPR up to a concentration of 10 μM.

Table 1. Initial SAR around Bicyclic Hit 1[a]

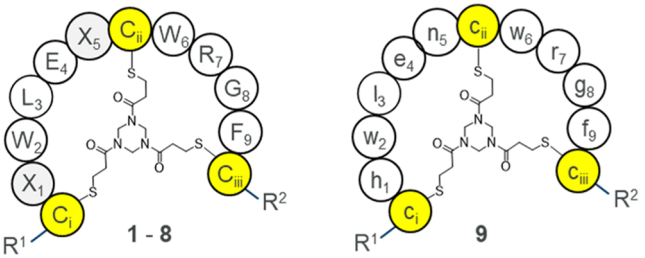

bicycle	R^1	X_1	X_5	R^2	K_D (nM)[b] hTSLP
1	A	H	N	A	230
2	A	Q	D	A	75
3	A	Q	D	ADGDML	29
4	A	Q	D	PLD	43
5	GTDSAE	Q	D	A	33
6	TMEYRD	Q	D	A	48
7	CH_3CO	H	N	NH_2	290
8	CH_3CO	Q	D	NH_2	98
9	CH_3CO	h	n	NH_2	>10,000

[a]IC_{50} values are the mean of two or more independent determinations. [b]Binding affinity of Bicycles to immobilized human TSLP determined by SPR.

Investigation of the Binding Mode and Analysis of the TSLP-Bicycle Interaction. To elucidate the binding mode of these hits, we first performed a series of SPR experiments. Bicycle **7** was found to bind to immobilized TSLP with the same affinity in the absence and presence of the TSLPR (Figure 2a), suggesting a binding site other than the TSLP−TSLPR interaction surface. Direct competition with IL-7Rα was not possible due to the poor affinity between TSLP and IL-7Rα in the absence of TSLPR, which is consistent with published data.[23] However, the binding of compound **7** could be outcompeted by the presence of both TSLPR and IL-7Rα (Figure 2a). These results suggested that **7** and its analogues might be binding to the IL-7Rα interaction surface.

Further proof for this hypothesis was obtained from hydrogen−deuterium exchange mass spectrometry (HDX-MS).[36−38] Here, we compared the TSLP protein in the presence and absence of compounds **1** and **7** and plotted the differential deuterium uptake onto the published X-ray structure of TSLP (Figure 2b).[22] Decreased hydrogen−deuterium exchange, indicating stabilization or protection from solvent, was observed at helices αA (residues 38−53) and αC (residues 98−106) at the TSLP:IL17Rα interface for both compounds (data shown for **7**). No significant changes in deuterium uptake were noted away from these regions.

Final confirmation of the binding site came from X-ray crystallographic studies. We obtained a co-crystal structure of compound **7** bound to human TSLP, the first reported structure of a small peptide binding to TSLP. The Bicycle could be unambiguously assigned and was indeed binding to the IL-7Rα binding site (Figure 3a). Bicycle **7** can be traced from Cys_i to Cys_{iii}, whereas its *N*- and *C*-termini were disordered. The covalent bonds between Cys_i, Cys_{ii}, and Cys_{iii} and the TATA moiety could be clearly assigned (Figure 3b). The carbonyl oxygens are pointing in the same, clockwise orientation when viewed from the top. The backbone NH

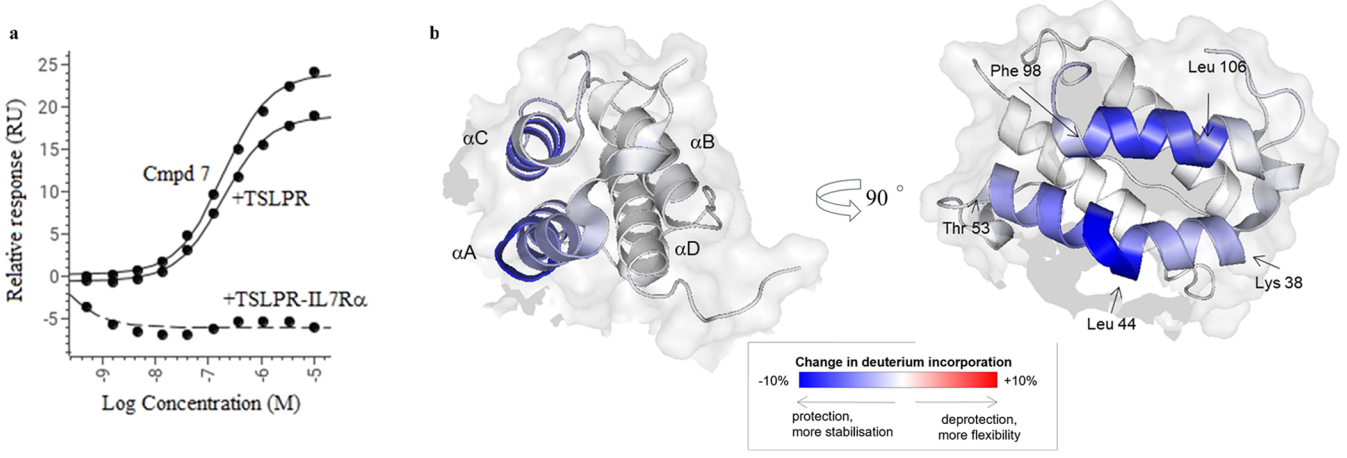

Figure 2. (a) Binding of compound **7** to immobilized hTSLP in dose−response, alone and in the presence of 3 μM TSLPR or 0.3 μM TSLPR-IL-7Rα (1:1 mix). (b) Differential deuterium uptake (TSLP + **7** versus TSLP alone) plotted onto the X-ray structure of TSLP (PDB 5J11).[22] Deeper shades of blue indicate greater ligand-induced stabilization.

https://doi.org/10.1021/acs.jmedchem.3c02163
J. Med. Chem. XXXX, XXX, XXX−XXX

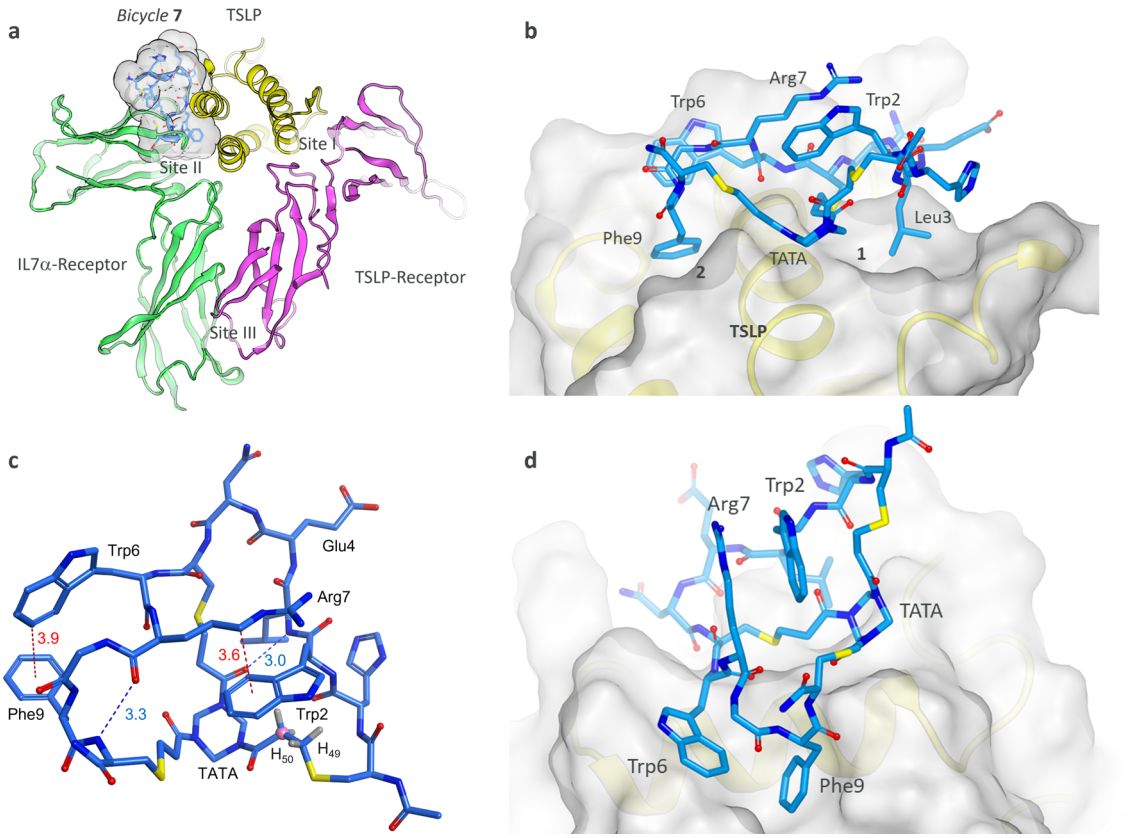

Figure 3. (a) X-ray structure of 7 (in blue with surrounding surface) bound to TSLP (yellow) (PDB 8QFZ, 1.65 Å), overlaid onto the structure of the trimeric signaling complex from PDB4NN7with IL-7Rα shown in green and the TSLPR in pink.[2,3] The binding site of 7 overlaps with site II on TSLP (IL-7Rα binding site) and is distal to site I (TSLPR binding site). (b) Binding site view of 7 and TSLP. (c) Bound structure of 7 with internal hydrogen-bonding and hydrogen−π interaction distances in Å. (d) Close-up view of subpocket 2. More detailed views are available in the SI (Figures S2a−d).

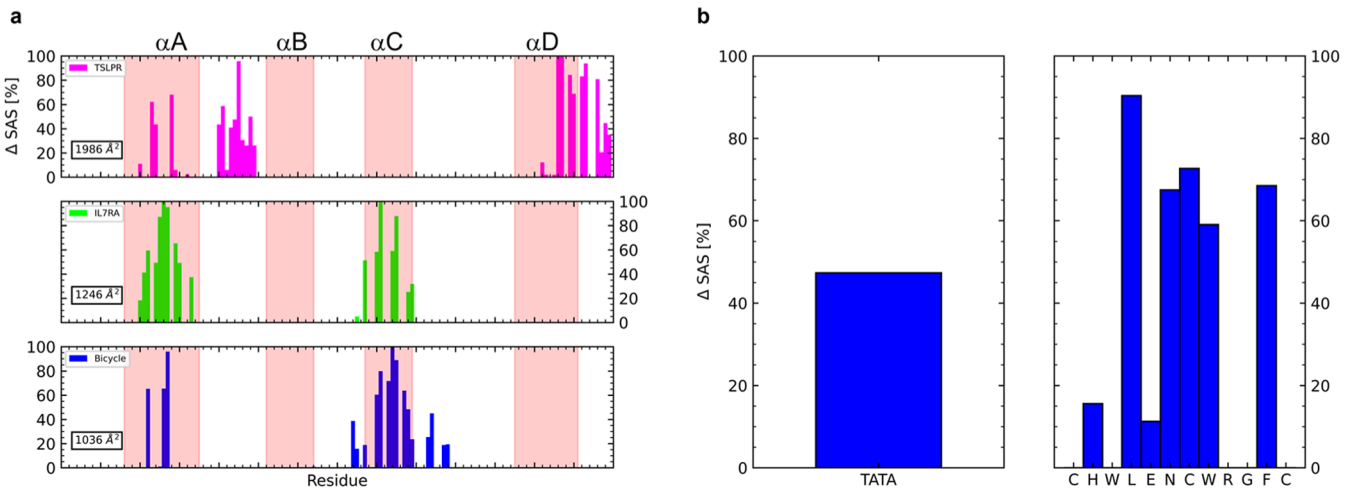

Figure 4. (a) TSLP residues involved in the PPI interfaces with TSLPR, IL-7Rα, and 7. The regions highlighted in red correspond to TSLP α-helices (A−D). (b) Residues of Bicycle 7 involved in the PPI interface with TSLP. The bars display ΔSAS[%] as defined in the General Methods section. A value of zero identifies residues not involved in the PPI; a value of 100 arises when the residue is completely buried at the interface. Values between 0 and 100 indicate the percentage of the solvent-accessible surface of the residue that is buried in the interface.

group of Leu3 and one of the three carbonyl groups of the TATA core are directly H-bonded, which might determine the direction of the TATA amide groups observed in the bound structure. Another intramolecular hydrogen bond is observed between NH of the C-terminal Cys_{iii} and the backbone carbonyl of Arg7. Arg7 does not participate in interactions with TSLP, but instead engages in an intramolecular stacking interaction with Trp2 above the plane of the Bicycle, thus stabilizing its bioactive conformation. The side chains of Leu3 and Phe9 of 7 are involved in hydrophobic interactions in two distinct subpockets of TSLP, designated as 1 and 2 here. Between these two subpockets, the TATA moiety is stacking

https://doi.org/10.1021/acs.jmedchem.3c02163
J. Med. Chem. XXXX, XXX, XXX−XXX

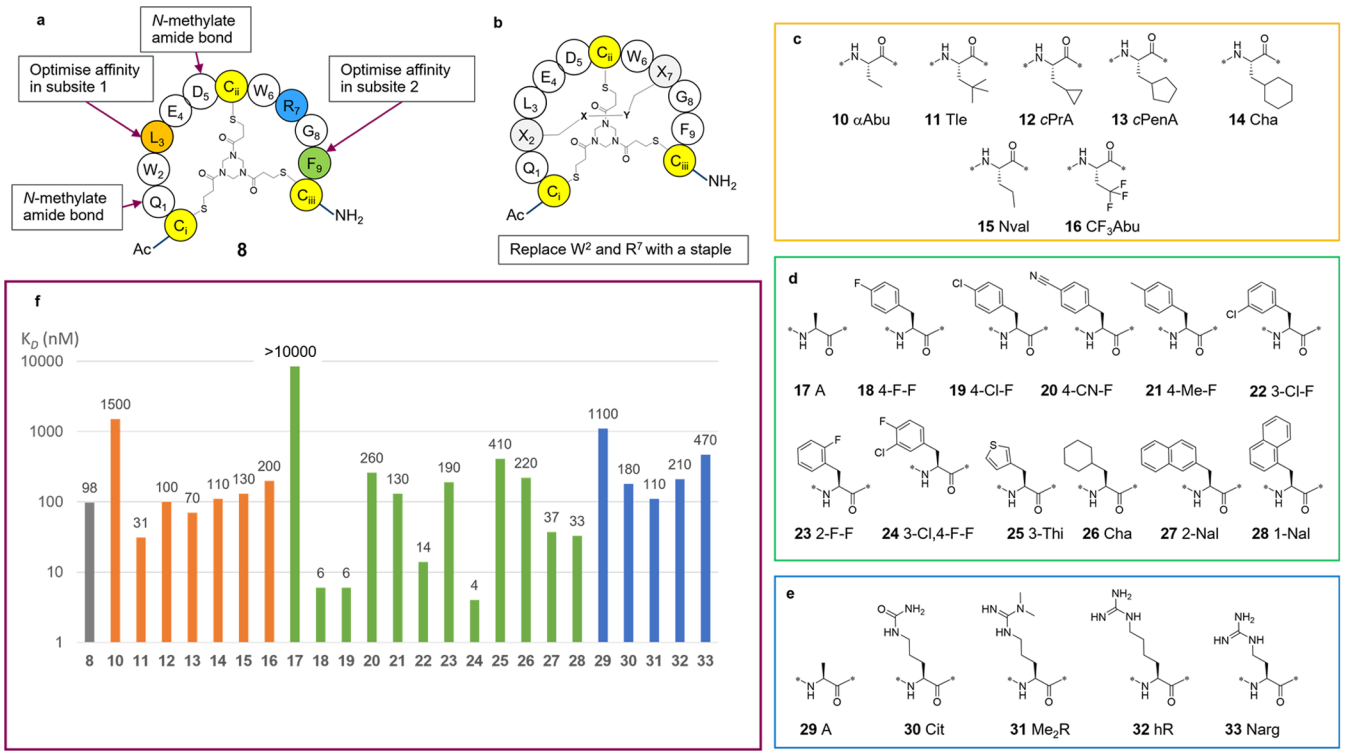

Figure 5. (a) Structure of **8** with amino acids initially investigated in orange (Leu3), green (Phe9), and blue (Arg7). (b) Structure of a bespoke tricyclic peptide, where Trp2 and Arg7 are replaced by a chemical staple. (c–e) Structures of amino acids introduced as single substitutions in **8** for Leu3 (c, orange), Phe9 (d, green), or Arg7 (e, blue). (f) Dissociation constants (K_D in nM, numbers above bars, *y*-axis in logarithmic scale) for peptides bearing a single substitution compared to **8** (gray bar); colors of bars correspond to color of amino acids in (a). Values were determined by SPR in at least two independent experiments.

onto TSLP. Interestingly, subpocket 2 is also the site that forms a major interaction with IL-7Rα, where the residue corresponding to Phe9 is Ile102 (see Supporting Information, Figure S1). We speculate that this site is a binding hotspot both for IL-7Rα and compound **7**.[23]

Apart from geometric complementarity between bound **7** and the binding site of TSLP, there are specific stabilizing H-bonding, $\pi-\pi$, and cation$-\pi$ intermolecular interactions between **7** and TSLP. The backbone carbonyl of Glu4 and the side-chain amino group of Lys103 are hydrogen-bonded. The backbone carbonyl of Asn5 seems to be involved in water-mediated H-bonding with the backbone carbonyl of Ala94. The amide NH group of Trp6 engages in an H-bond to the backbone carbonyl of Met100, and its indole moiety participates in a stacking interaction with Lys10. It is also involved in a $\pi-\pi$ edge-to-face interaction with Phe9, which in its turn is close to the side chain of Trp109 from TSLP.

We calculated the solvent-accessible surface areas (SAS) of TSLP and its different interaction partners using the published structure of the human signaling complex and our own structure.[22] Bicycle **7** has the smallest footprint of these three (interface area 1036 Å^2), with the interface for IL-7Rα (1246 Å^2) and TSLPR (1986 Å^2) being significantly larger. In addition, the two receptors also interact with each other in the membrane proximal region, where another 780 Å^2 are buried (Site III in Figure 3a).[22] There are also fewer residues of TSLP involved in the interaction with Bicycle **7** compared to both receptor chains (Figure 4a). The TSLP receptor not only gives the largest interface area but also gives the most extensive interface involving helices A and D, the loop connecting helices A and B, and the C-terminal loop. The IL-7 receptor α chain and **7** share the same TSLP epitope, involving helices A and C, although in a different fashion. IL-7Rα interacts with more residues on helix A while the Bicycle interacts with more residues on helix C and involves the connecting loops of the helix, both N- and C-terminal to it. Figure 4b details the interaction of the bicyclic peptide with TSLP. The TATA scaffold also contributes to the interface, burying 50% of its solvent-accessible surface in the interaction. The leucine residue is almost fully buried in the interface, as is the central cysteine and phenylalanine.

Improvement of Binding Affinity and Proteolytic Stability. Bicycle **7** was characterized further for stability in human and rat plasma and rat and human lung S9 fractions. It was stable in rat plasma, with 90% of parent compound remaining after 2 h, but rapidly disappeared from rat and human lung S9 fraction with a half-life of less than 5 min. Bicycle **9**, the enantiomer of **7**, which is completely composed of D-amino acids, was stable under these conditions, indicating that proteolysis was the main reason for the instability of **7** in lung preparations.

To improve the potency and proteolytic stability of this series we relied on the information provided by the X-ray structure of **7** bound to TSLP. The side chains of Leu3 and Phe7 were targeted to maximize the interactions in subpockets 1 and 2 and two amide bonds in loop 1, in positions 1 and 5 were identified for *N*-methylation (Figure 5a). In the bound structure of **7**, these NH protons point toward bulk solvent and are not involved in intra- or intermolecular interactions (see SI, Figure S2a). In a second approach, we envisioned replacing the π–cation interaction between Trp2 and Arg7 above the bicyclic plane with a stable chemical linkage, which we

https://doi.org/10.1021/acs.jmedchem.3c02163
J. Med. Chem. XXXX, XXX, XXX−XXX

Table 2. SAR around Lead Peptide 18[a]

	sequence									
bicycle	1	2	3	4	5	6	7	9	R	K_D (nM)[b] hTSLP
18	Q	W	L	E	D	W	R	4−F−F	NH_2	6
34	Q	W	Tle	E	D	W	R	4−F−F	NH_2	3
35	Q	W	L	E	D	W	R	4−F−F	OH	33
36	Q	W	L	E	D	W	R	4−F−F	a	14
37	Q	W	L	Q	D	W	R	4−F−F	NH_2	6
38	Q	W	L	Q	D	W	Me_2R	4−F−F	NH_2	9
39	MeA	W	L	E	D	W	Me_2R	4−F−F	NH_2	13
40	Q	2Nal	L	E	D	W	Me_2R	4−F−F	NH_2	20
41	Q	2Nal	L	E	D	W	Me_2R	4−F−F	a	36
42	Q	NMeW	Tle	E	D	NMeW	Me_2R	4−F−F	NH_2	3
43	MeA	NMeW	Tle	Q	D	NMeW	Me_2R	4−F−F	NH_2	6
44	MeA	NMeW	Tle	Q	MeD	NMeW	Me_2R	4−F−F	NH_2	3
45	Q	NMeW	Tle	Q	D	NMeW	Me_2R	3-Cl-4−F−F	NH_2	2
46	MeA	2Nal	Tle	Q	D	NMeW	Me_2R	4−F−F	a	13

[a]K_D values are the mean of two or more independent determinations. [b]Binding affinity determined by SPR of compounds to immobilized human TSLP.

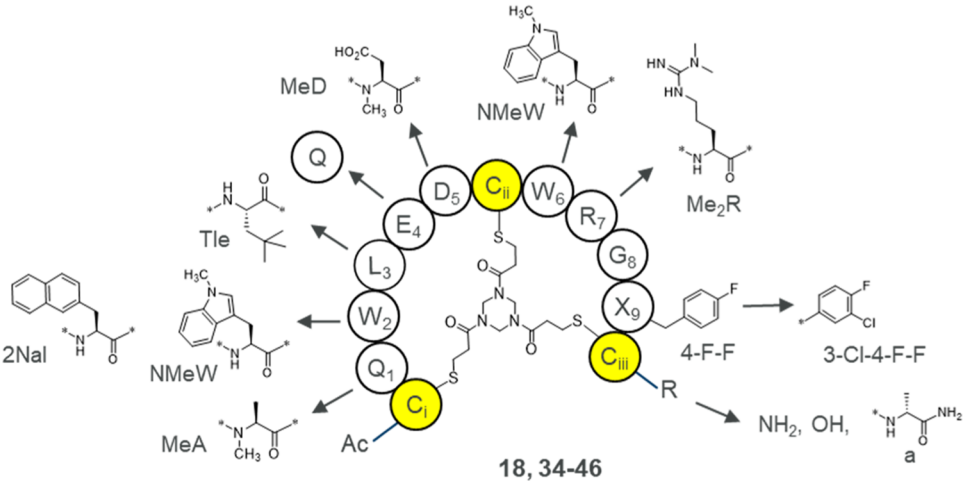

Figure 6. Modifications around lead peptide **18**. Positions and amino acids used are indicated by arrows. Results are shown in Table 2.

hypothesized would stabilize the resulting compound against proteolytic cleavage (see Figure 5b).

We used the higher-affinity compound **8** as the starting point. Figure 5 shows the SAR around **8** obtained by introducing single amino acid substitutions. For Leu3, a 15-fold loss in affinity was observed upon removal of the branching methyl groups, whereas a 3-fold increase was realized by adding an additional methyl group. Several other hydrophobic side chains were also accepted but were less optimal compared to *tert*-butylalanine (Figure 5c,f).

In loop 2, the conversion of Phe9 to Ala resulted in a greater than 100-fold loss of binding affinity, highlighting the importance of this residue for the interaction with TSLP. The introduction of fluorine or chlorine in the *para*-position of the aromatic ring of Phe9 improved affinity by around 15-fold (**18** or **19**, K_D = 6 nM), whereas methyl or cyano residues led to a slight loss in affinity. In the *meta*-position, the introduction of chlorine also resulted in a significant affinity gain, but not as pronounced as in the *para*-position. A clear loss was observed by the introduction of fluorine in the *ortho*-position. Combining halogen substitution in the *meta*- and *para*-position, as in **24** (K_D = 4 nM), did not yield a significant improvement. Based on the available SAR, we believe that the introduction of the halogen atom makes the phenyl ring sufficiently electron-poor to act as the optimal partner between the stacking interactions with Trp109 of TSLP and Trp2 of the Bicycle. Replacement of the phenyl ring with either cyclohexyl or thienyl led to a 2- to 4-fold loss in affinity, whereas both naphthyl isomers were accepted, leading to peptides that were about 3-fold better than **8**.

We also investigated the SAR around the arginine residue. Conversion of Arg7 to Ala worsened affinity by an order of magnitude, whereas removal of the charge using isosteric citrulline resulted only in a 2-fold loss (**30**, K_D = 180 nM), showing that the interaction with Trp2 in loop 1 is mainly hydrophobic in nature. Elongation or shortening of the side chain, as well as *N,N*-dimethylation, as in analogues **31**-**33**, were also accepted. Combination of the best residues in positions 3 and 9 led to a 30-fold improvement in affinity over **8** (**34**, K_D = 3 nM, Table 2).

At this stage, early data on the metabolism of Bicycle **7** in rat lung homogenate was obtained. In addition to nearly complete removal of loop 1, conversion of the C-terminal amide to the acid was observed as the major metabolite. Consequently, we prepared the parent acid of **18** and observed a 5-fold loss in affinity (**35**, K_D = 33 nM, Table 2). A more favorable

https://doi.org/10.1021/acs.jmedchem.3c02163
J. Med. Chem. XXXX, XXX, XXX−XXX

modification was identified by capping the C-terminus with D-alanine (**36**, K_D = 14 nM).

Subsequently, we introduced several non-natural amino acids in loops 1 and 2 of **18** (Figure 6) to investigate their effect on proteolytic stability. These changes were largely based on the X-ray structure of **7** bound to TSLP and included the introduction of bulkier side chains in positions 2, 3, 6, and 7, the exchange of Glu4 to Gln, as well as the *N*-methylation of the amide backbone in positions 1 and 5. Most of these changes did not impact the affinity significantly compared to **18** (Table 2). For example, exchanging Glu4 for Gln was well tolerated (**37**, K_D = 6 nM), since only Asp5 engages in the ionic interaction with Lys95 of TSLP. Compound **38** shows that bulkier Me_2Arg can be used in position 7 instead of Arg. The replacement of Gln1, where neither its side chain nor its amide backbone seem to interact with TSLP, with *N*-methyl-alanine (**39**, K_D = 13 nM) was also tolerated. Several of these changes were combined and with Tle in position 3 instead of Leu led to the potent analogues **42**−**45** with K_D values between 2 and 6 nM. In Bicycle **44**, Asp5 was replaced with its *N*-methyl derivative without loss in affinity, compared to **43**. Several of these compounds were further evaluated in rat lung S9 fraction, and these results are discussed below.

For the tricyclic structure, several potential linking groups, replacing the Arg7 and Trp2 side chains, were modeled and an olefinic or alkyl linkage composed of six atoms gave the best fit (Table 3). Scheme 1 describes the synthesis for analogues **51**−**53**. We prepared the resin-bound peptide **47**, where the side chains of Trp2 and Arg7 were replaced with 4-butenyl residues and transformed into Bicycle **48** after cleavage from the resin. The ring-closing metathesis (RCM) reaction on **48** was tried under a variety of conditions but gave the desired tricyclic peptide only in low yield and purity. Conducting the RCM reaction directly on the resin to give the resin-bound peptide **49** led to better overall yields.[39] After cleavage from the resin, **49** could be cyclized with TATA to give the tricycles as a mixture of the *cis*- and *trans* isomers **51** and **52**, which were separated by RP-HPLC. The saturated analogue **53** was derived in an analogous manner from **50**, obtained by hydrogenation of resin-bound **49**.

Table 3. SPR Data for Bicycles 18 and 48 and Tricycles 51-55 and Results from DFT Calculations for Selected Tricycles with Respect to 18[a]

peptide	X−X	K_D (nM)[b] hTSLP	RMDS C_α [Å][c]	AA2C_α-AA7C_α [Å][d]
18	n.a.	6	0.0	8.17
48	n.a.	900		
51	(*Z*)−CH=CH−	52	0.70	7.24
52	(*E*)−CH=CH−	97	0.46	7.69
53	$-(CH_2)_2-$	77	0.78	7.26
54	$-(CH_2)_3-$	664		
55	$-(CH_2)_4-$	82	1.05	7.35

[a]K_D values are the mean of two or more independent determinations. [b]Binding affinity to immobilized human TSLP determined by SPR. [c]Root-mean-square deviation (RMSD) between locations of the 12 C_α-carbons of Bicycle **18** and the tricycles. For **18**, we assumed the same binding mode as observed for **7**. [d]C_α−C_α—distance between C_α carbons of Trp2 and Arg7 for **18** or between the beginning and the end of the stapling chain for the tricycles.

Compound **48** itself was 150-fold less potent with respect to **18**, evidencing the importance of the Trp-Arg interaction for the bioactive conformation of the Bicycle (Table 3). An approximate 10-fold improvement in affinity with respect to **48** was realized upon cyclization to the analogues **51**−**53**. Based on the coupling constant of J = 8 Hz for the olefinic protons, we assigned the *Z*-configuration to the double bond present in **51**.

We then explored the chain length of the alkyl tether, starting from the appropriate olefinic precursors (see the Supporting Information), and found that extending the linkage by one carbon led to a 10-fold loss in affinity (**54**, K_D = 664 nM), whereas extension by two carbons was tolerated (**55**, K_D = 82 nM).

Overall, analogues **51**−**53** did not reach the affinity of **18**, remaining 10- to 16-fold less active. Unfortunately, we were unable to obtain the X-ray co-crystal structure of a tricyclic analogue bound to TSLP to see the impact of the staple on its conformation with respect to Bicycle **18**. Based on density functional theory (DFT) calculations, the staple does not fully mimic the original interaction, as can be seen by the deviation of the α-carbons of the tricycles and the shorter distance between the α-carbons of position 2 and 7 with respect to **18** (Table 3). We chose to investigate potential differences in the conformations of **18** and **51** by NMR spectroscopy. The best quality proton spectra of **18**, judged by separation of signals and minimal broadening, was obtained at 278 K in aqueous solution with pH and ionic strength mimicking physiological conditions. An almost complete assignment of the proton spectrum could be made through a combination of TOCSY, HSQC, and NOESY spectra (see SI, Figure S3 and Tables S3 and S4). NH temperature coefficients were consistent with H-bonding from the C-terminal cysteine NH to the backbone carbonyl of Arg7 as observed in the bound crystal structure (see Figures 7 and 3c). However, there was no evidence from temperature coefficients for the H-bond from Leu3 to one of the scaffold carbonyls that is observed in the crystal. This is likely because of an exchange occurring in solution between different amide rotamers. In fact, we observed two conformations that exchange slowly on the NMR time scale at room temperature in the proton NMR spectrum in an approximate ratio of 1:8. This is consistent with the presence of two predominant amide rotamers.

NOEs were observed from the Trp2 aromatic proton H62 (orange) to all of the arginine protons H93 to H96 (orange dots) and from H63 (gray) to the TATA scaffold H50 (see Figure 7). These are consistent with observed distances in the crystal structure. Additional long-distance NOEs were observed, which are also consistent with the interactions observed in the X-ray structure. Of interest is an anomalous shielding for the scaffold protons (H49′/H49″ and H50′/H50″) compared to the equivalent protons in the other two scaffold groups. These appear at 1.18 and 2.06 ppm (H49) compared to 2.84 and 2.94 and 1.33 and 1.46 ppm (H50) compared to 2.74 and 2.89 ppm. This shielding effect is consistent with these protons lying under the plane of the tryptophan ring as observed in the crystal and shown in Figure 3c.

The NMR data of tricycle **51** were determined in an analogous manner and showed good agreement, both with regards to the long-range NOE interactions seen and hydrogen-bonding interactions evidenced by the NMR temperature coefficients with the structure of **18** (see SI

https://doi.org/10.1021/acs.jmedchem.3c02163
J. Med. Chem. XXXX, XXX, XXX−XXX

Scheme 1. Synthesis of Bicyclic Peptide 48 and Tricyclic Peptides 51−53[a]

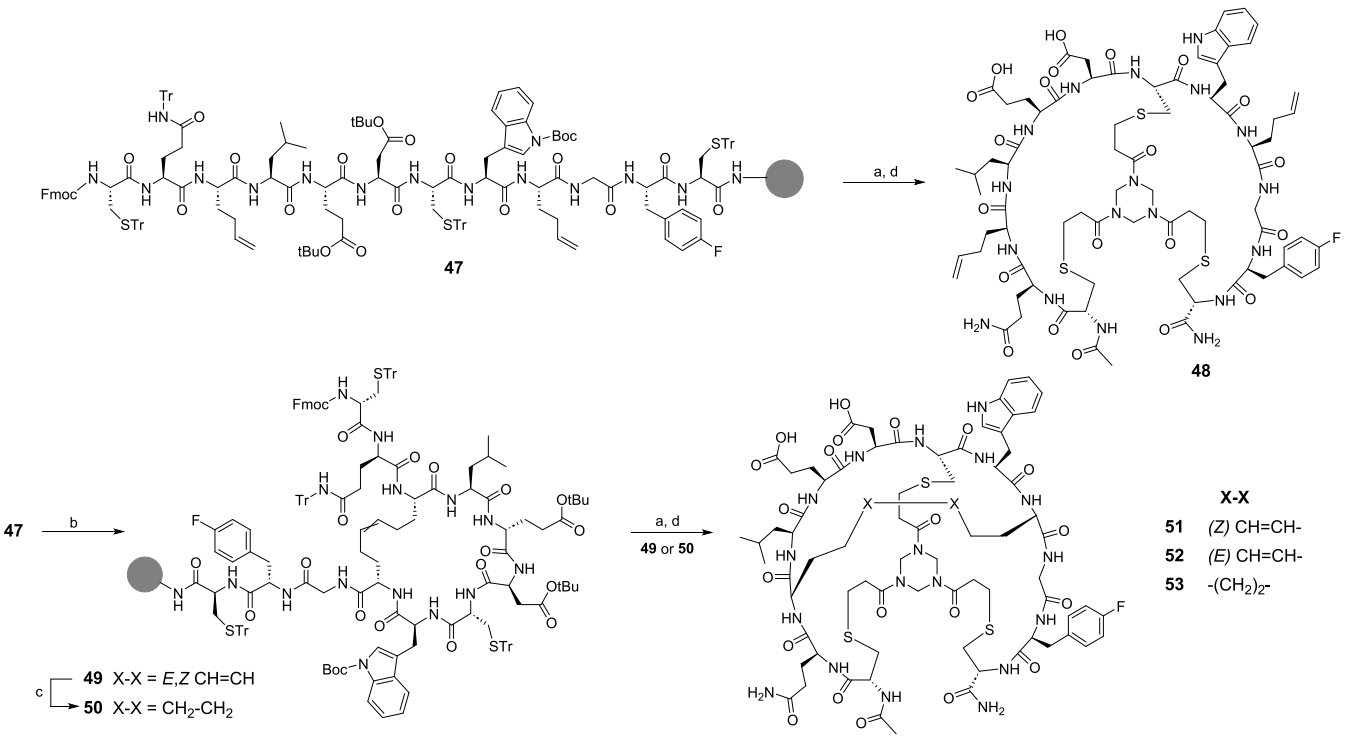

[a]Reagents and conditions: (a) 20% piperidine, DMF; Ac_2O, iPr_2NEt, TFA, iPr_3SiH, H_2O, DODT, 2.5 h; (b) benzylidene-bis(tricyclohexylphosphine)dichlororuthenium, DCM 40 °C, 24 h; (c) $[RhCl(PPh_3)_3]$, H_2 (4 bar), DCM:MeOH (9:1), 40 °C, 24 h; (d) TATA, MeCN, H_2O, rt, 1 h.

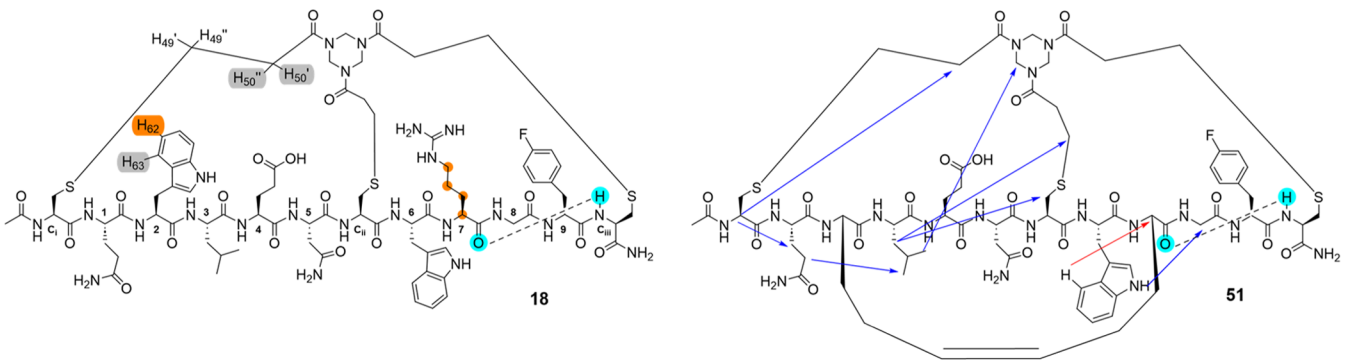

Figure 7. Comparison of NMR structures of **18** and **51**. Specific NOEs for **18** are depicted and described in the text. Long-range NOEs, observed in **18** and **51**, are indicated with blue arrows in the structure of **51**. The red arrow in structure **51** indicates an NOE, which is present in **18** and absent in **51**. NOEs observed between Trp2 proton H62 (labeled in orange) and Arg7 protons (H93 to H96, orange dots). NOEs observed between Trp2 proton H63 and TATA scaffold protons H50′ & H50″ (gray labels). C_{iii} backbone NH and Arg7 backbone carbonyl (cyan circles) form H-bond (dashed line). The numbering of the peptide backbone in **51** has been omitted for clarity.

Tables S5 and S6). All of the NOEs between remaining residues and from residues to scaffold that were observed in **18** were also observed in **51**, as indicated by blue arrows in Figure 7, except for an NOE from the remaining Trp6 to the adjacent α proton at the site of attachment of the linker (red arrow). It is not surprising that the conformation in this region is adjusted. In common with **18**, there is no evidence for an H-bond from Leu3 to the scaffold. The NH temperature coefficient of F-phenylalanine is higher in the tricycle suggesting that this NH proton is more solvent-accessible compared to the Bicycle. Overall, from these observations, we concluded that the conformation of the tricycle was similar to that of the Bicycle **18** and assumed the same binding mode for both compounds.

Encouraged by the gain in potency observed for some of the analogues in Table 2, we tested several of them for inhibition of TSLP signaling in human peripheral blood mononuclear cells (PBMCs). PBMCs isolated from healthy donors were stimulated with TSLP to induce production of CCL17. A commercial human TSLP antibody was able to completely inhibit CCL17 production with low nanomolar potency (see SI, Figure S4). We tested some of our most potent compounds using two different concentrations of TSLP for stimulation (50 and 400 pM), and in both cases observed inhibition of CCL17 production only at the highest concentration of 10 μM. This is

https://doi.org/10.1021/acs.jmedchem.3c02163
J. Med. Chem. XXXX, XXX, XXX−XXX

about 1000-fold above their respective affinities for TSLP (Figure 8). The tested compounds were found to be stable under the assay conditions.

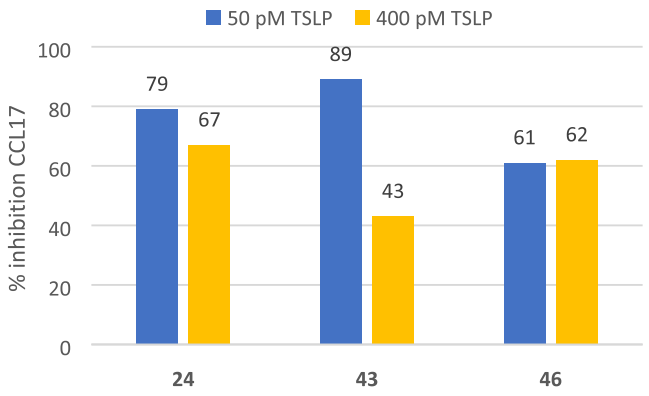

Figure 8. Inhibition of TSLP signaling measured as inhibition of production of CCL17 in human PBMCs stimulated with either 50 (blue) or 400 (yellow) pM TSLP. Bicycles were tested at a fixed concentration of 10 μM.

The absence of activity is maybe not that surprising, based on what is known about TSLP signaling and the signaling of IL-2 cytokines in general.[40] Mechanistically, it has been shown that TSLP first interacts with TSLPR at site I to form a high-affinity complex. Complex formation induces allosteric activation of TSLP, and only the dimeric complex can recruit IL-7Rα to site II with high affinity (see also Figure 4a). The affinity of TSLP alone to IL-7Rα is in the micromolar range, as we also have confirmed.[23] Based on the binding mode of our compounds, which bind to site II, also in the presence of TSLPR (Figure 1), we hypothesize that a TSLP-Bicycle complex can bind to TSLPR on the receptor surface. Despite good affinity, as determined by SPR, the Bicycle is not potent enough to prevent the recruitment of IL-7Rα. The formation of the ternary signaling complex is not only governed by the interactions in site II, where the Bicycle forms a smaller interaction surface, as shown in Figure 4, but also by the interaction between the extracellular membrane-proximal domains of the two receptors, which covers an extensive surface area.

To better understand this behavior, we investigated by SPR whether the Bicycles could inhibit the formation of the trimeric complex composed of TSLP and both receptors.

First, we determined kinetic parameters for the initial Bicycle **7** and its optimized analogue **43** (Table 4). Notably, **7** with a 30-fold weaker affinity than **43** has only a 2-fold slower on-rate, whereas the off-rate was 14-fold faster. In other words, the improvement in affinity is mostly derived from an improved off-rate. Furthermore, the fast on-rate ($\sim 10^6$ M^{-1} s^{-1}) suggests that Bicycles adopt a preformed structure that subsequently docks onto TSLP. This is also consistent with the NMR studies, which support the existence of well-defined conformations.

Table 4. Kinetic Parameters for Selected Bicycles[a]

bicycle	K_D (M)	k_{on} (M^{-1} s^{-1})	k_{off} (s^{-1})
7	2.2×10^{-7}	4.8×10^{5}	9.3×10^{-2}
43	6.4×10^{-9}	1.1×10^{6}	6.9×10^{-3}
fold difference	30	2.3	14

[a]Values are the mean of at least seven measurements. The difference in K_D for **7** vs Table 1 is due to steady state versus kinetic curve fit.

We then reconstituted the trimeric signaling complex by immobilizing IL-7Rα on the SPR chip and flowing over a fixed concentration of TSLP−TSLPR complex. The addition of increasing concentration of **7** or **43** or soluble IL-7Rα showed inhibition of complex formation in a dose-dependent manner. IL-7Rα was significantly more potent than the Bicycles at preventing ternary complex formation (Figure 9a and Table 5). Similarly, when we reconstituted the trimeric signaling complex by immobilizing TSLPR on the SPR chip and flowing over fixed concentrations of TSLP and IL-17Rα, the addition of increasing concentration of **7** or **43** showed inhibition of complex formation in a dose-dependent manner. Here, TSLPR was significantly more potent than the Bicycles (Figure 9b). This supports our hypothesis that blocking site II alone is likely insufficient to outcompete the formation of the ternary complex, which involves additional contact sites at the membrane proximal regions.

Pharmacokinetic Evaluation. Delivery via the lung poses different challenges for peptides versus parenteral routes, such as retention in the lung and exposure to proteases.[41,42] To establish whether Bicycles could be optimized for lung delivery, we investigated the pharmacokinetic (PK) properties of our compounds and evaluated a selection for stability in rat lung S9 fractions and rat plasma. For a subset, we also determined the pharmacokinetic parameters after intravenous or intratracheal administration (Table 6).

All compounds in Table 6 were tested for stability in rat plasma and shown to be stable with >50% recovered following 18 h incubation in rat plasma (data not shown). However, significant differences were noted in rat S9 fractions using a recently established protocol.[43,44] Here, D-peptide **9** was stable, but Bicycle **18**, as well as the tricycles **52** and **53**, demonstrated short half-lives of 34 to 48 min. The C-terminal acid **35** and especially its D-Ala analogue **36** showed improved terminal $t_{1/2}$ compared to **18**. We were able to identify some major metabolites for compounds **35** and **52**. For **35**, complete removal of loop 1 was observed, together with another major metabolite, which still had Asp5 attached (Figure 10). For tricycle **52**, three major metabolites, all formed in loop 1, were identified. The aliphatic staple in **52** prevented complete loss of loop 1, confirming our initial hypothesis that a staple replacing the Arg7 and Trp2 interaction would increase stability, but led only to a minor improvement in these cases, and further modifications in loop 1 would have been necessary.

Bulkier side chains in positions 2 and 7, as in analogue **40**, provided more stable compounds compared to **18**. This stability was further improved by the introduction of the C-terminal D-Ala as in **41**. Analogues **42**, **43**, and **45**, with Tle in position 3 in loop, showed enhanced stability, which again was further improved by capping with D-Ala as in **46**. The improved stability observed by the introduction of non-natural amino acids provided additional improvement to the pharmacokinetics after intravenous dosing.

The plasma PK of **9** was characterized by low clearance, in line with expected renal elimination of the peptide. About 64% of parent compound **9** could be recovered in rat urine, and after IT dosing, a long mean residence time (MRT) in lung of >24 h and a lung bioavailability of 34% were observed. The plasma PK of Bicycle **35** and **36**, and tricycle **52** was substantially inferior to **9**, characterized by high plasma clearance and short effective half-life of 2 to 5 min. The D-

https://doi.org/10.1021/acs.jmedchem.3c02163
J. Med. Chem. XXXX, XXX, XXX−XXX

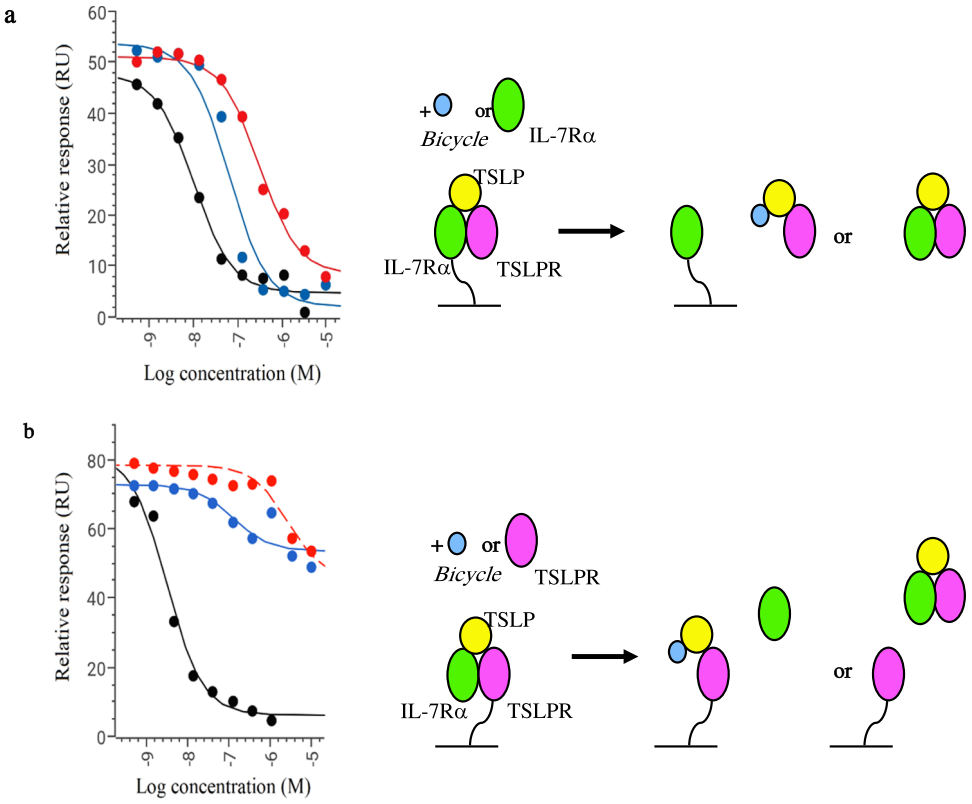

Figure 9. Comparison of SPR dose−response curves showing disruption of TSLP−TSLPR-IL-7Rα ternary complex formation. (a) Increasing concentrations of **7** (red), **43** (blue), and free IL-7Rα (black), in the presence of a fixed concentration of TSLP and TSLPR, with IL-7Rα immobilized as shown in the schematic. (b) Increasing concentrations of **7** (red), **43** (blue), and free TSLPR (black), in the presence of a fixed concentration of TSLP and IL-7Rα, with TSLPR immobilized as shown in the schematic. The difference in baseline levels is due to the fact that TSLP still binds to the TSLPR on the chip in the presence of the bicyclic peptides, whereas the free TSLPR sequesters free TSLP.

Table 5. Inhibition of Complex Formation[a]

bicycle/protein	IC_{50} (nM) IL-7Rα immob.	fold difference vs IL-7Rα	IC_{50} (nM) TSLPR immob.	fold difference vs TSLPR
7	320	32	2800	900
43	63	6.3	130	42
IL-7Rα	10	1.0		
TSLPR			3.1	1.0

[a]Values are the mean of two independent measurements.

Ala capping group in **36** did not provide any advantage compared to the parent amide **35**, despite showing better stability in rat lung S9 fraction. For **52**, only a small portion of the dose could be recovered unchanged in urine. The D-Ala containing analogue **41**, having bulkier side chains in position 2 in loop 1 and position 7 in loop 2, showed a reduction in plasma clearance and a slightly improved $t_{1/2}$.

Plasma clearance was significantly reduced in analogues **42**, **45**, and **46** containing Tle in position 3 of loop 1. For **42**, clearance was lowered, and $t_{1/2}$ extended to nearly half an hour. Bicycles **45** and **46** showed even lower CL values and improved half-lives, like the D-analogue **9**. However, recovery of intact compound in rat urine remained significantly lower than for **9**, pointing to broad metabolism instead of passive or active renal clearance.

The significant improvements in plasma PK translated only partially to improvements in IT PK. Compared to D-peptide **9**, with an MRT of >24 h and 34% of compound reaching the circulation, most of compounds achieved MRTs of 1−2 h. However, the compounds with the highest density of non-natural amino acids and with good lung S9 and low plasma clearance (e.g., **42**, **45**, and **46**) delivered more parent compound to the circulation and had better MRT when compared to analogues **35**, **36**, and **52**.

These results show that proteolytic stability in plasma and lung of this series could be significantly improved, and further improvements beyond those described here are certainly feasible.

Conclusions. In conclusion, we describe the identification of a series of potent Bicycles binding to TSLP, a cytokine involved in the pathogenesis of type 2 asthma and a variety of other diseases. Binding to TSLP is demonstrated by using biophysical methods and ultimately by an X-ray co-crystal structure of **7** bound to TSLP. To our knowledge, these are the only small peptide binders to this cytokine. This crystal structure shows that **7** binds to a hotspot also used by IL-7Rα, and this information was utilized to further optimize affinity and proteolytic stability. This extensive chemistry campaign focused on the lipophilic interactions in the binding hotspots, stabilization of the bioactive conformation, and the introduction of non-natural amino acids. Several of these modified Bicycles reached single-digit nanomolar affinity to TSLP and demonstrated low plasma clearance as well as good effective half-life after intravenous dosing, comparable to the pharmacokinetics observed for a non-active analogue composed entirely of D-amino acids. Overall, these results show that Bicycles can drug sites of protein−protein interactions on challenging therapeutic targets that are hard to address with

https://doi.org/10.1021/acs.jmedchem.3c02163
J. Med. Chem. XXXX, XXX, XXX−XXX

Table 6. Stability of Bicyclic and Tricyclic Peptides in Rat Lung S9 Fraction and Pharmacokinetic Parameters after Intravenous (IV) and Intratracheal (IT) Dosing to Male Han Wistar Rats

		IV Rat PK[b]				IT dosing to the lung[b]	
peptide	$t_{1/2}$ rat lung S9 (min)[a]	CL (mL/min/kg)	V_{ss} (L/kg)	effective $t_{1/2}$ (min)	parent in urine (%)	F(%)	lung MRT (h)
9	stable	6.3	0.60	66	64	33.9	>24
18	35						
35	67	45	0.13	2		2.3	1.0
36	144	42	0.30	5		3.4	1.2
40	83						
41	stable	23	0.23	7	0.3	8.6	2.2
42	stable	12	0.42	26	1.0	24.7	1.3
43	143						
45	92	6.4	0.32	35	0.8	22.5	1.8
46	stable	6.4	0.41	45	0.9	23.0	2.4
52	48	46	0.21	3	0.1	5.9	0.5
53	34						

[a]Peptides were incubated in rat lung S9 and half-lives determined as described previously; stable denotes >75% of parent compound present at the 60 min time point. [b]Male Han Wistar rats (n = 2) were dosed intravenously via a jugular vein catheter with the peptides at doses ranging from 0.6 to 2.0 μmol/kg in PBS containing 5% EtOH at dose volumes of 4 mL/kg or intratracheally at dose volumes of 2 mL/kg. They were kept in metabolic cages to be able to collect urine samples. Non-compartmental analysis of plasma and lung samples was conducted to determine PK parameters (CL, V_{ss}, Lung MRT, F%) and effective $t_{1/2}$ (0.693 × V_{ss}/CL).

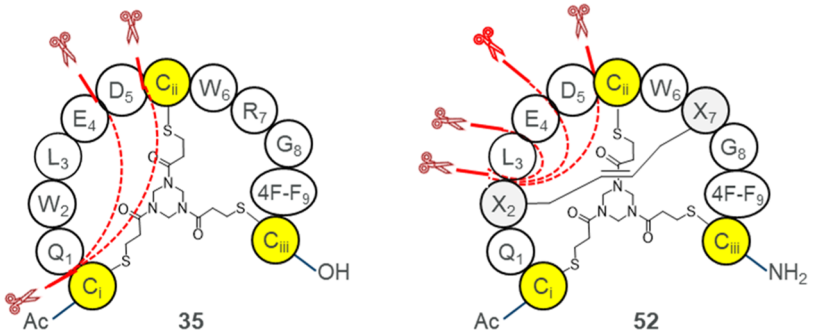

Figure 10. Structures of compounds **35** and **52** with major sites of metabolism, identified by LC-MS, shown by red lines.

small molecules and that affinity and pharmacokinetic properties can be optimized.

Experimental Section. *General Methods.* NMR spectra were recorded on a Bruker Avance III spectrometer at a proton frequency of 500 or 600 MHz. The central peaks of chloroform-δ (H 7.26 ppm), CD_3OD (H 3.30 ppm), or DMSO-d_6 (H 2.50 ppm) were used as internal references. Liquid chromatography-mass spectrometry (LCMS) experiments were performed using a Waters Acquity system combined with a Waters Xevo Q-ToF Mass in ESI mode. HRMS (high-resolution mass spectrometry) was run on a high-resolution (R = 9000 fwhm) LCMS system (Waters Acquity−Xevo Q-ToF) with electrospray ionization (ESI). Preparative HPLC was performed with a Waters FractionLynx system with integrated MS detection or Gilson GX-281 with integrated UV detection using a variety of columns. Examples are Waters Sunfire C18 OBD5 μm 19 mm × 150 mm or 30 mm × 150 mm, XBridge BEH C18 OBD 5 μm 19 mm × 150 mm or 30 mm × 150 mm, Xselect CSH C18 OBD 5 μm 19 mm × 150 mm or Chromasil C8 10 μm 20 mm × 250 mm or 50 mm × 250 mm columns.

General Solid-Phase Peptide Synthesis. Peptides were synthesized as previously described, and this is described below and exemplified with the preparation of **44** and **46**.[35] The synthesis of the tricycles is available in the Supporting Information, together with characterization data and HPLC traces for selected compounds. Compounds were isolated at ≥90% purity by HPLC.

General Peptide Synthesis. Linear peptides were synthesized by solid-phase peptide synthesis (SPPS), based on Fmoc chemistry, using one of the following peptide synthesizers: Symphony, manufactured by Peptide Instruments, Biotage Initiator + Alstra and Syro II from Biotage and Liberty Blue from CEM. Rink Amide ChemMatrix resin (100−200 mesh) from Biotage with a loading of around 0.5 mmol/g was used unless otherwise stated. Standard Fmoc amino acids were employed with the following side chain protecting groups: Arg(Pbf) or Arg(Boc)$_2$; Asn(Trt); Asp(O^{t}Bu); Cys(Trt); Glu(O^{t}Bu); Gln(Trt); His(Trt); Lys(Boc); Ser(tBu); Thr-(^{t}Bu); Trp(Boc); and Tyr(^{t}Bu). Standard Fmoc amino acids, as well as nonproteinogenic Fmoc amino acids, were obtained from Sigma-Aldrich, Iris Biotech GmbH, Apollo Scientific, ChemImpex, and Fluorochem. The preparation of 4-Chloro-*N*-{[(9*H*-fluoren-9-yl)methoxy]carbonyl}-3-fluoro-L-phenylalanine is described above.

Cleavage and deprotection of the linear peptides from the resin was carried out as follows: A solution of trifluoroacetic acid (TFA)/triisopropylsilane (TIS)/3,6-dioxa-1,8-octanedithiol (DODT)/water (92.5:2.5:2.5:2.5, 90:2.5:2.5:5, or 95:2.5:0:2.5 vol/vol, 5−20 mL) was added to the dried resin. The reaction was vortexed at rt for 2−4 h. The resin was removed by filtration and washed with DCM (3 × 10 mL),

https://doi.org/10.1021/acs.jmedchem.3c02163
J. Med. Chem. XXXX, XXX, XXX−XXX

MeOH (3 × 10 mL), and again with DCM (3 × 10 mL). The volume of the combined filtrates was reduced to 10−20 mL, and the peptides were precipitated with ice-cold Et_2O or MTBE (20−40 mL). The mixture was centrifuged, the liquid decanted off, and the sediment resuspended in cold ether, and centrifuged again. This process was repeated two more times. Typically, the linear peptides were used without further purification in the TATA cyclization step.

Cyclization of Linear Peptides with TATA. 1,3,5-Triacryloyl-1,3,5-triazinane (TATA, 1 equiv), dissolved in MeCN (2−4 mL), and aqueous NH_4HCO_3 buffer (0.06 M, pH 7.9, 10−20 mL) were added to a solution of the crude linear peptide (10−200 mg) in a mixture of MeCN (8−16 mL) and water (10−20 mL). The reaction was stirred at rt for 2−24 h and monitored by LCMS. Typically, the reaction was quenched with HCO_2H (0.5−2 mL), but this step could also be omitted. Subsequently, the mixture was filtered, the filtrate was freeze-dried, and the resulting crude product was purified by RP-HPLC. Peptide fractions of sufficient purity and the correct molecular weight (verified by LC−MS) were pooled and lyophilized.

Following trifluoroacetic acid-based cleavage from the resin, peptides were precipitated with diethyl ether and dissolved in 50:50 acetonitrile/water. The crude peptides (at ∼1 mM concentration) were then cyclized with 1.3 equiv of TATA scaffold, using ammonium bicarbonate (100 mM) as a base. Completion of cyclization was determined by matrix-assisted laser desorption ionization time-of-flight (MALDI-TOF) or liquid chromatography−mass spectrometry (LC−MS). Once complete, the cyclization reaction was quenched using N-acetyl cysteine (10 equiv with respect to TATA), and the solutions were lyophilized. The residue was dissolved in an appropriate solvent and purified by reversed-phase (RP) HPLC. Peptide fractions of sufficient purity and the correct molecular weight (verified by either MALDI-TOF and HPLC or LC−MS) were pooled and lyophilized. Concentrations were determined by UV absorption using the extinction coefficient at 280 nm, which was based on Trp/Tyr content.

Preparation of 44. Step 1: Preparation of Ac-Cys-(NMe-Ala)-(NMe-Trp)-(^{t}Bu-Ala)-Gln-Asp-Cys-(NMe-Trp)-(dimethyl-Arg)-Gly-(4-F-Phe)-Cys-NH_2. The linear peptide was prepared on a 0.2 mmol scale on the Biotage Initiator + Alstra to give 215 mg (66%). LCMS (Acquity CSH C18 1.7 μm, pH 3, rt 6.02 min, 20 to 60% MeCN in 10 min): ES^+ 819.3 $[M + 2H]^{2+}$.

Step 2: TATA cyclization. The linear peptide was cyclized to yield the title compound (29 mg, 19%) after purification by preparative HPLC (column: Waters Atlantis T3 ODB 5 μm 150 mm × 19 mm; mobile phase: A − H_2O/TFA 100:0.15 and B − MeCN with a gradient 5% B for 0.5 min, 5−33% B in 1.5 min, 33−38% B in 14 min; flow 30 mL/min at rt, detection 230 nm). HRMS: calcd for $(C_{86}H_{119}FN_{22}O_{19}S_3 + 2H)^{2+}$ 940.4162; found (ESI $[M + 2H]^{2+}$) 940.4159, purity 93%.

Preparation of 46. Step 1: Preparation of *C*-(NMe-Ala)-(1-naphthyl-Ala)-(^{t}Bu-Ala)-Q-D-C-(NMe-Trp)-(dimethyl-Arg)-*G*-(4-F-Phe)-C-*a*-NH_2. The linear peptide was prepared, following the general procedure on 730 mg rink amide resin (0.35 mmol, 0.48 mmol/g). Cleavage and deprotection from the resin were performed with a mixture of TFA (20 mL), water (1.5 mL), TIS (0.8 mL), and 0.8 mL of DODT (0.8 mL) over 4 h. The resin was filtered off and washed with DCM (3 × 10 mL) and MeOH (3 × 10 mL). The volume of the filtrate was reduced in vacuo to around 20 mL, and the peptide was precipitated by adding a mixture of heptane-MTBE 1:1 v/v (100 mL). After centrifugation, the liquid was decanted and the sediment was resuspended in a mixture of heptane-MTBE and centrifuged again. The residue was dissolved in a mixture of MeCN-water 1:1 (ca. 100 mL) and lyophilized to give the linear peptide (463 mg, 80%). LCMS (Acquity CSH C18 1.7 μm, pH 3, rt 1.10 min, 10 to 90% MeCN in 4 min): ES^+ m/z = 830.3 $[M + 2H]^{2+}$, purity 82%.

Step 2: TATA cyclization. The foregoing linear peptide (463 mg, 0.28 mmol) was dissolved in a mixture of MeCN (95 mL), water (100 mL), and 60 mM NH_4HCO_3 buffer (60 mM, 100 mL) under nitrogen atmosphere. TATA (69.7 mg, 0.28 mmol), dissolved in MeCN (5 mL) was added portionwise over ca. 3 min. The resulting mixture was stirred for 1 h at rt, acidified with formic acid (4 mL), and freeze-dried. The residue was subjected to preparative RP-LC (Column: Chromasil C-18 5 cm × 100 cm, mobile phase: A—H_2O/TFA (0.2% TFA) and B—MeCN with a gradient of 10−60% B in 30 min, flow rate 100 mL/min) to afford the title compound (99 mg, 17%). HRMS: calculated for $(C_{88}H_{121}FN_{22}O_{19}S_3 + 2H)^{2+}$ 953.4240; found (ESI $[M + 2H]^{2+}$) 953.4250.

Surface Plasmon Resonance (SPR) Binding Assay. Biotinylated human TSLP was immobilized on a streptavidin-coated biosensor chip (GE Healthcare or XanTec Bioanalytics GmbH). Typical capture levels were 500−2000 response units (RU). Buffer conditions were 50 mM HEPES pH 7.4, 150 mM NaCl, 0.005% (v/v) Tween20, and 1% DMSO. Peptides were flowed over surface in 7 or 10 concentration−response series. Typical contact times were 60 s followed by 180−600 s dissociation. Sensorgrams were analyzed using the SPR-module of Genedata Screener and fit either with a steady-state or kinetic 1:1 binding model depending on affinity regime.

SPR Competition Experiments. Mechanism of action competition studies were carried out using TSLP, TSLPR, or IL-7Rα immobilized biosensor chips.

Immobilized TSLP. TSLP was immobilized as described above. The effect of peptide binding in the presence of 3 μM TSLPR or 0.3 μM TSLPR-IL-7Rα (1:1 mix) was monitored. Direct competition experiments with the IL-7Rα were not performed since IL-7Rα alone does not bind TSLP.

Immobilized IL-7 Receptor α. IL-7Rα was immobilized using amine coupling onto CM5 chips (GE Healthcare). The surface was activated with *N*-hydroxysuccinimide and *N*-ethyl-*N*′-(dimethylaminopropyl) carbodiimide. IL-7Rα was diluted to 0.3 μM in acetate buffer pH 5.0 and injected. Typical capture levels were around 500 response units. TSLP and TSLPR were preincubated together at 30 nM and added to each well containing increasing amounts of peptide or free IL-7Rα. Steady-state response levels were measured by subtracting the signal corresponding to only the TSLP−TSLPR complex.

TSLP-Receptor Immobilized. TSLP receptor was immobilized using amine coupling onto CM5 chips (GE Healthcare). The surface was activated with *N*-hydroxysuccinimide and *N*-ethyl-*N*′-(dimethylaminopropyl) carbodiimide. TSLPR was diluted to 1 μM in acetate buffer pH 4.5 and injected. Capture levels were around 500 response units. TSLP and IL-7Rα were preincubated at 10 nM and added to each well containing increasing amounts of peptide or free TSLPR. Steady-state response levels were measured by subtracting the

https://doi.org/10.1021/acs.jmedchem.3c02163
J. Med. Chem. XXXX, XXX, XXX−XXX

signal corresponding to that obtained when injecting only TSLP and IL-7Rα.

Hydrogen−Deuterium Exchange Mass Spectrometry (HDX-MS). TSLP (Thr28-Gln159) was used in all experiments. 20 μM apo TSLP was preincubated with 5× excess of ligand or equal volume of DMSO for 30 min. Exchange reactions were performed with a CTC PAL sample handling robot (LEAP Technologies). Reactions were conducted by incubating 3 μL of TSLP with 57 μL of D_2O buffer (containing 20 mM Tris-HCl (pH 7.9), 20 mM NaCl) for times of 0.5, 1, 10, and 30 min. The exchange reaction was stopped by the addition of 50 μL of quench solution (2 M Urea, 1 M TCEP). The sample was injected onto an online pepsin digestion system and subjected to pepsin digestion using a BEH pepsin column (Waters) 2.1 mm × 30 mm in 0.3% formic acid in water at 200 $\mu Lmin^{-1}$ and trapped the digested peptide using a 2.1 mm × 5 mm, 1.7 μm, C18 trap (ACQUITY UPLC BEH C18 VanGuard Pre-Column, Waters) column for 3 min. The resulting desalted peptides were separated and eluted using C18 reversed-phase column (ACQUITY UPLC BEH C18 Column, 1.7 μm, 2.1 mm × 100 mm, Waters) with a 6 min 5−40% acetonitrile (containing 0.1% formic acid) gradient at 40 $\mu Lmin^{-1}$. The resulting peptides were ionized by electrospray onto a SYNAPT G2-Si mass spectrometer (Waters) acquiring in MSE mode for detection and mass measurements. Peptides from an unlabeled protein were identified using ProteinLynx Global Server searches of a protein database including analyte protein. Each deuterium labeling experiment was performed in at least triplicate.

Relative deuterium levels for each peptide were calculated by subtracting the average mass of the deuterium-labeled sample from that of the nondeuterated control sample. All mass spectra were processed with DynamX 3.0 (Waters). The data normalization was calculated with in-house software written in MATLAB (Mathworks). The structural representations of hydrogen−deuterium exchange data were represented using Pymol and the HDX−MS data were calculated using the mean deuteration level per amino acid, as reported.[45]

TSLP-Bicycle 7 Crystallization. Human 6xHN-tagged-TSLP at a concentration of 12 mg/mL in 20 mM Tris pH 7.5 and 200 mM NaCl was mixed with 5× molar excess of **7** dissolved in DMSO. The mixture was incubated at room temperature for 1 h and spun down 10 min before broad crystal screening was performed. Crystals were obtained in the Morpheus screen (Molecular Dimensions) in condition G9:30% PEG MME 500/PEG 20,000, 0.1 M carboxylic acids mix, and 0.1 M buffer system 3 pH 8.5. Crystals were flash-frozen in liquid nitrogen without the addition of any cryoprotection, and data was collected at beamline ID30B at the European Synchrotron Radiation Facility, France.

The structure was solved using molecular replacement (Molrep).[46] The coordinates of the TSLP molecule from the ternary structure of the TSLP−TSLP-receptor-IL-7-receptor α complex (PDB ID: 5J11)[22] were used as a search model. After refinement using the program REFMAC,[47] the structure of **7** could be unambiguously assigned in the electron density (see Table S7 in the Supporting Information). All modeling and structure building was carried out using Coot.[48] The final structure exhibits excellent geometry (RMSD bonds, 0.02 Å; angles, 2.2°). The structure has been deposited in the PDB (PDB code 8QFZ).

Calculations of Solvent-Accessible Surface (SAS). The solvent-accessible surface (SAS) calculations were performed with the FreeSASA package, version 2.0.3 (Simon Mitternacht (2016) FreeSASA: An open-source C library for solvent-accessible surface area calculation. F1000Research 5:189 (doi: 10.12688/f1000research.7931.1)) as a python module. The Lee and Richards algorithm was used with the default 1.4 Å probe radius. High resolution was achieved by setting the parameter n-slices equal to 100; only heavy atoms were considered. The coordinates for each of the systems (Tezepelumab complex (RCSB PDB 5J13), ternary receptor complex (RCSB PDB 5J11),[22] and the complex of **7** with TSLP (this work)) were prepared with Maestro 2022−4 from Schrödinger. Missing side chains and missing loops were constructed with Prime.

The interface area of two interacting proteins, schematically identified as A and B was obtained as

$$\text{area}_{\text{Interface}} = (\text{SAS}_{\text{A}} + \text{SAS}_{\text{B}} - \text{SAS}_{\text{AB}}) \quad (1)$$

where SAS_A and SAS_B are the solvent-accessible surface of the isolated components not in contact with each other. This was achieved by making separate coordinate files for protein A and protein B. SAS_{AB} is the solvent-accessible surface of the complex, calculated using the coordinates of the complete system.[49]

Residues involved in the protein−protein interaction were identified by calculating

$$\Delta\text{SAS}[\%] = 100 \times \frac{(\text{SAS}_{\text{isolated}} - \text{SAS}_{\text{complex}})}{\text{SAS}_{\text{isolated}}} \quad (2)$$

Two solvent-accessible surface calculations were performed, one of the isolated protein of interest, TSLP, or the bicyclic peptide, for example, and an additional one of the protein of interest in the complex. The results of the calculations were split into residue contributions. If a residue is not involved in the interface the numerator of eq 2 will be zero as the result from both calculations will be identical; normalizing to the values coming from the calculation of the isolated system allows comparison between different systems. In summary, ΔSAS[%] varies between 0, i.e., residue not involved in the protein−protein interface, and 100, i.e., residue totally buried at the interface ($SAS_{complex} = 0$).

Human Peripheral Blood Mononuclear Cell Assay. Human peripheral blood mononuclear cells (PMBCs) were obtained from heparinized whole blood (2 healthy donors) by density gradient centrifugation using Lymphoprep (StemCell Technologies, Vancouver, BC) according to the manufacturer's instructions. The PBMCs were washed twice with PBS containing 2 mM EDTA and 2% fetal calf serum (FCS) and reconstituted in RPMI containing 10% FCS and 2% PenStrep at a final concentration of 10 million cells/mL. This cell suspension (100 μL) was aliquoted into the wells of a 96-well flat-bottom tissue culture plate. 5 μL of Bicycle peptide or vehicle (0.1% DMSO in complete medium) was then added and mixed into the cells. The plate was incubated for 30 min in a 10% CO_2, humidified incubator at 37 °C. 5 μL of TSLP or vehicle (complete medium) was then added and mixed to the cells. The final concentration in the assay was 50−400 pM TSLP and 10−0.123 μM peptide. The plate was incubated for 24 h in a 10% CO_2 and humidified incubator at 37 °C. The plate was centrifuged at 300*g* for 5 min, and the collected supernatants were frozen at −20 °C for subsequent CCL17/TARC and CCL22/MDC analysis.

https://doi.org/10.1021/acs.jmedchem.3c02163
J. Med. Chem. XXXX, XXX, XXX−XXX

CCL17/TARC was determined by MSD (MesoScale Discovery, Maryland) according to the manufacturer's instructions. Percent inhibition was calculated by dividing the mean of the peptide-treated sample for both donors by the mean of the vehicle group for both donors.

Rat Lung S9 Incubations. The stability of the peptides was assessed in rat lung S9 using an automated assay as described in our previous publication.[43,44] Briefly, peptides were incubated at 10 μM in freshly prepared rat lung S9 (from frozen male Wistar Han lungs) diluted to a protein concentration of 5 mg/mL. All stability incubations were run on a Hamilton STAR automated liquid handling robot. Rat lung S9 was plated and preincubated at 37 °C for 15 min before the experiments were initiated by the addition of 5 μL of peptide stock. All stability incubations were conducted in triplicate and the half-lives reported are the mean of the 3 values generated. As in our previous study, a peptide was considered stable if >75% of starting material was detected at the 60 min time point. For all other peptides, half-life values were calculated as compiled in Table 6.

Rat PK Studies. Test system male Wistar Han rats from Charles River France at an ordering weight of 250−275 g were allowed to acclimatize for at least 5 days before start of the study. The rats were housed in cages (5 animals per cage) with hard wood shavings from Tapvei (Finland), as bedding material and environmental enrichment, like nest pads and gnaw sticks. They were kept at 21 ± 1 °C, and at a relative humidity of 55 ± 15% during a 12 h light/dark cycle with free access to food and water.

■ ASSOCIATED CONTENT

Supporting Information

The Supporting Information is available free of charge at https://pubs.acs.org/doi/10.1021/acs.jmedchem.3c02163.

Experimental procedures and characterization data for final compounds, crystal structure data, and HPLC traces (PDF)

Molecular formula strings (SMILES) (CSV)

Accession Codes

The atomic coordinates and structure factors for compound 7 (PDB code 8QFZ) are deposited in the Protein Data Bank and will be released upon publication

■ AUTHOR INFORMATION

Corresponding Author

Frank Narjes − *Medicinal Chemistry, BioPharmaceuticals R&D, AstraZeneca, 431 50 Gothenburg, Sweden;* orcid.org/0000-0002-3104-7771; Phone: +46 706468373; Email: Frank.Narjes@astrazeneca.com

Authors

Fredrik Edfeldt − *Mechanistic & Structural Biology, R&D, AstraZeneca, Gothenburg SE-431 83, Sweden*

Jens Petersen − *Mechanistic & Structural Biology, R&D, AstraZeneca, Gothenburg SE-431 83, Sweden*

Linda Öster − *Mechanistic & Structural Biology, R&D, AstraZeneca, Gothenburg SE-431 83, Sweden*

Corinne Hamblet − *Bioscience, Research & Early Development, Respiratory & Immunology, BioPharmaceuticals R&D, AstraZeneca, 431 50 Gothenburg, Sweden*

James Bird − *DMPK, BioPharmaceuticals R&D, AstraZeneca, 431 50 Gothenburg, Sweden*

Peter Bold − *DMPK, BioPharmaceuticals R&D, AstraZeneca, 431 50 Gothenburg, Sweden*

Rebecca Rae − *Medicinal Chemistry, BioPharmaceuticals R&D, AstraZeneca, 431 50 Gothenburg, Sweden*

Elisabeth Bäck − *Bioscience, Research & Early Development, Respiratory & Immunology, BioPharmaceuticals R&D, AstraZeneca, 431 50 Gothenburg, Sweden*

Stina Stomilovic − *DMPK, BioPharmaceuticals R&D, AstraZeneca, 431 50 Gothenburg, Sweden*

Pavol Zlatoidsky − *Medicinal Chemistry, BioPharmaceuticals R&D, AstraZeneca, 431 50 Gothenburg, Sweden*

Tor Svensson − *Medicinal Chemistry, BioPharmaceuticals R&D, AstraZeneca, 431 50 Gothenburg, Sweden*

Lotta Hidestål − *Medicinal Chemistry, BioPharmaceuticals R&D, AstraZeneca, 431 50 Gothenburg, Sweden*

Lavaniya Kunalingam − *Medicinal Chemistry, BioPharmaceuticals R&D, AstraZeneca, 431 50 Gothenburg, Sweden*

Igor Shamovsky − *Medicinal Chemistry, BioPharmaceuticals R&D, AstraZeneca, 431 50 Gothenburg, Sweden;* orcid.org/0000-0002-2881-9531

Leonardo De Maria − *Medicinal Chemistry, BioPharmaceuticals R&D, AstraZeneca, 431 50 Gothenburg, Sweden;* orcid.org/0000-0002-8061-4242

Euan Gordon − *Protein Science, Discovery Science, R&D, AstraZeneca, Gothenburg SE-431 83, Sweden*

Richard J. Lewis − *Medicinal Chemistry, BioPharmaceuticals R&D, AstraZeneca, 431 50 Gothenburg, Sweden;* orcid.org/0000-0001-9404-8520

Sophie Watcham − *BicycleTx Limited, Portway Building, Cambridge CB21 6GS, U.K.*

Katerine van Rietschoten − *BicycleTx Limited, Portway Building, Cambridge CB21 6GS, U.K.;* orcid.org/0000-0002-0360-8244

Gemma E. Mudd − *BicycleTx Limited, Portway Building, Cambridge CB21 6GS, U.K.;* orcid.org/0000-0002-5075-1625

Helen Harrison − *BicycleTx Limited, Portway Building, Cambridge CB21 6GS, U.K.*

Liuhong Chen − *BicycleTx Limited, Portway Building, Cambridge CB21 6GS, U.K.;* orcid.org/0000-0003-1776-3146

Michael J. Skynner − *BicycleTx Limited, Portway Building, Cambridge CB21 6GS, U.K.*

Complete contact information is available at: https://pubs.acs.org/10.1021/acs.jmedchem.3c02163

Author Contributions

The manuscript was written through contributions of all authors. All authors have given approval to the final version of the manuscript.

Notes

The authors declare the following competing financial interest(s): The authors are employees of either AstraZeneca or Bicycle Therapeutics (or were at the time this work was carried out) and may own stock or stock options.

■ ACKNOWLEDGMENTS

The authors thank their colleagues in the analytical and separation science team at Gothenburg for the purification of

https://doi.org/10.1021/acs.jmedchem.3c02163
J. Med. Chem. XXXX, XXX, XXX−XXX

the peptides and analytical support and the peptide chemistry team at Bicycle Therapeutics for the preparation of the phage-identified Bicycles. They acknowledge early contributions of Jenny Gunnarsson, Sarah Dorbeus, Stefan Tångefjord, Edmond Wong, James Hunt, Jennifer Hicks Silvio Di Castro, and Johan Wernevik from Discovery Sciences, and from Suman Mitra and Matthew Catley from R&I BioScience.

■ ABBREVIATIONS USED

Ac, acetyl; CCL17, CC chemokine ligand 17; CL, clearance; DCM, dichloromethane; DFT, density functional theory; DMF, dimethylformamide; DMSO, dimethyl sulfoxide; DODT, 3,6-dioxa-1,8-octanedithiol; ESI, electrospray ionization; F, bioavailability; HDX-MS, hydrogen−deuterium exchange mass spectroscopy; HPLC, high-performance liquid chromatography; IL, interleukin; IV, intravenous; IT, intratracheal; LC-MS, liquid chromatography−mass spectrometry; MTBE, methyl *tert*-butyl ether; MRT, mean residence time; NOE, nuclear Overhauser effect; NMR, nuclear magnetic resonance; PBS, phosphate buffer solution; PK, pharmacokinetics; PPI, protein−protein interaction; rt, room temperature; SAR, structure−activity relationship; SAS, solvent-accessible surface area; SPR, surface plasmon resonance; TATA, 1,3,5-triacrolyl-1,3,5-triazinane; TFA, trifluoroacetic acid; TSLP, thymic stromal lymphopoietin; TSLPR, thymic stromal lymphopoietin receptor; V_{ss}, Volume of distribution

■ REFERENCES

(1) D'Aloisio, V.; Dognini, P.; Hutcheon, G. A.; Coxon, C. R. Peptherdia: Database and Structural Composition Analysis of Approved Peptide Therapeutics and Diagnostics. *Drug Discovery Today* **2021**, *26*, 1409−1419.
(2) Muttenthaler, M.; King, G. F.; Adams, D. J.; Alewood, P. F. Trends in Peptide Drug Discovery. *Nat. Rev. Drug Discovery* **2021**, *20*, 309−325.
(3) Wang, L.; Wang, N.; Zhang, W.; Cheng, X.; Yan, Z.; Shao, G.; Wang, X.; Wang, R.; Fu, C. Therapeutic Peptides: Current Applications and Future Directions. *Signal Transduction Targeted Ther.* **2022**, *7*, No. 48.
(4) Shultz, M. D. Two Decades under the Influence of the Rule of Five and the Changing Properties of Approved Oral Drugs. *J. Med. Chem.* **2019**, *62*, 1701−1714.
(5) Goto, Y.; Suga, H. The Rapid Platform for the Discovery of Pseudo-Natural Macrocyclic Peptides. *Acc. Chem. Res.* **2021**, *54*, 3604−3617.
(6) Morrison, C. Constrained Peptides' Time to Shine? *Nat. Rev. Drug Discovery* **2018**, *17*, 531−533.
(7) Robertson, N.; Spring, D. Using Peptidomimetics and Constrained Peptides as Valuable Tools for Inhibiting Protein−Protein Interactions. *Molecules* **2018**, *23*, No. 959.
(8) Zorzi, A.; Deyle, K.; Heinis, C. Cyclic Peptide Therapeutics: Past, Present and Future. *Curr. Opin. Chem. Biol.* **2017**, *38*, 24−29.
(9) Vinogradov, A. A.; Yin, Y.; Suga, H. Macrocyclic Peptides as Drug Candidates: Recent Progress and Remaining Challenges. *J. Am. Chem. Soc.* **2019**, *141*, 4167−4181.
(10) Jiang, Z.; Guan, J.; Qian, J.; Zhan, C. Peptide Ligand-Mediated Targeted Drug Delivery of Nanomedicines. *Biomater. Sci.* **2019**, *7*, 461−471.
(11) Mudd, G. E.; Scott, H.; Chen, L.; van Rietschoten, K.; Ivanova-Berndt, G.; Dzionek, K.; Brown, A.; Watcham, S.; White, L.; Park, P. U.; Jeffrey, P.; Rigby, M.; Beswick, P. Discovery of Bt8009: A Nectin-4 Targeting Bicycle Toxin Conjugate for the Treatment of Cancer. *J. Med. Chem.* **2022**, *65*, 14337−14347.
(12) Lamers, C. Overcoming the Shortcomings of Peptide-Based Therapeutics. *Future Drug Discovery* **2022**, *4*, No. FDD75.
(13) Cazzola, M.; Ora, J.; Calzetta, L.; Rogliani, P.; Matera, M. G. The Future of Inhalation Therapy in Chronic Obstructive Pulmonary Disease. *Curr. Res. Pharmacol. Drug Discovery* **2022**, *3*, No. 100092.
(14) Mudd, G. E.; Brown, A.; Chen, L.; van Rietschoten, K.; Watcham, S.; Teufel, D. P.; Pavan, S.; Lani, R.; Huxley, P.; Bennett, G. S. Identification and Optimization of Epha2-Selective Bicycles for the Delivery of Cytotoxic Payloads. *J. Med. Chem.* **2020**, *63*, 4107−4116.
(15) Upadhyaya, P.; Lahdenranta, J.; Hurov, K.; Battula, S.; Dods, R.; Haines, E.; Kleyman, M.; Kristensson, J.; Kublin, J.; Lani, R.; Ma, J.; Mudd, G.; Repash, E.; Rietschoten, K. V.; Stephen, T.; You, F.; Harrison, H.; Chen, L.; McDonnell, K.; Brandish, P.; Keen, N. Anticancer Immunity Induced by a Synthetic Tumor-Targeted Cd137 Agonist. *J. Immunother. Cancer* **2021**, *9*, No. e001762.
(16) Harman, M. A. J.; Stanway, S. J.; Scott, H.; Demydchuk, Y.; Bezerra, G. A.; Pellegrino, S.; Chen, L.; Brear, P.; Lulla, A.; Hyvonen, M.; Beswick, P. J.; Skynner, M. J. Structure-Guided Chemical Optimization of Bicyclic Peptide (Bicycle) Inhibitors of Angiotensin-Converting Enzyme 2. *J. Med. Chem.* **2023**, *66*, 9881−9893.
(17) Ebina-Shibuya, R.; Leonard, W. J. Role of Thymic Stromal Lymphopoietin in Allergy and Beyond. *Nat. Rev. Immunol.* **2023**, *23*, 24−37.
(18) Soumelis, V.; Reche, P. A.; Kanzler, H.; Yuan, W.; Edward, G.; Homey, B.; Gilliet, M.; Ho, S.; Antonenko, S.; Lauerma, A.; Smith, K.; Gorman, D.; Zurawski, S.; Abrams, J.; Menon, S.; McClanahan, T.; Waal-Malefyt, Rd.; Bazan, F.; Kastelein, R. A.; Liu, Y.-J. Human Epithelial Cells Trigger Dendritic Cell−Mediated Allergic Inflammation by Producing Tslp. *Nat. Immunol.* **2002**, *3*, 673−680.
(19) Zhang, Y.; Zhou, B. Functions of Thymic Stromal Lymphopoietin in Immunity and Disease. *Immunol. Res.* **2012**, *52*, 211−223.
(20) Gauvreau, G. M.; Bergeron, C.; Boulet, L. P.; Cockcroft, D. W.; Cote, A.; Davis, B. E.; Leigh, R.; Myers, I.; O'Byrne, P. M.; Sehmi, R. Sounding the Alarmins-the Role of Alarmin Cytokines in Asthma. *Allergy* **2023**, *78*, 402−417.
(21) Gauvreau, G. M.; White, L.; Davis, B. E. Anti-Alarmin Approaches Entering Clinical Trials. *Curr. Opin. Pulm. Med.* **2020**, *26*, 69−76.
(22) Verstraete, K.; Peelman, F.; Braun, H.; Lopez, J.; Van Rompaey, D.; Dansercoer, A.; Vandenberghe, I.; Pauwels, K.; Tavernier, J.; Lambrecht, B. N.; Hammad, H.; De Winter, H.; Beyaert, R.; Lippens, G.; Savvides, S. N. Structure and Antagonism of the Receptor Complex Mediated by Human Tslp in Allergy and Asthma. *Nat. Commun.* **2017**, *8*, No. 14937.
(23) Verstraete, K.; van Schie, L.; Vyncke, L.; Bloch, Y.; Tavernier, J.; Pauwels, E.; Peelman, F.; Savvides, S. N. Structural Basis of the Proinflammatory Signaling Complex Mediated by Tslp. *Nat. Struct. Mol. Biol.* **2014**, *21*, 375−382.
(24) Diver, S.; Khalfaoui, L.; Emson, C.; Wenzel, S. E.; Menzies-Gow, A.; Wechsler, M. E.; Johnston, J.; Molfino, N.; Parnes, J. R.; Megally, A.; Colice, G.; Brightling, C. E. Effect of Tezepelumab on Airway Inflammatory Cells, Remodelling, and Hyperresponsiveness in Patients with Moderate-to-Severe Uncontrolled Asthma (Cascade): A Double-Blind, Randomised, Placebo-Controlled, Phase 2 Trial. *Lancet Respir. Med.* **2021**, *9*, 1299−1312.
(25) Gauvreau, G. M.; O'Byrne, P. M.; Boulet, L. P.; Wang, Y.; Cockcroft, D.; Bigler, J.; FitzGerald, J. M.; Boedigheimer, M.; Davis, B. E.; Dias, C.; Gorski, K. S.; Smith, L.; Bautista, E.; Comeau, M. R.; Leigh, R.; Parnes, J. R. Effects of an Anti-Tslp Antibody on Allergen-Induced Asthmatic Responses. *N. Engl. J. Med.* **2014**, *370*, 2102−2110.
(26) Menzies-Gow, A.; Corren, J.; Bourdin, A.; Chupp, G.; Israel, E.; Wechsler, M. E.; Brightling, C. E.; Griffiths, J. M.; Hellqvist, Å.; Bowen, K.; Kaur, P.; Almqvist, G.; Ponnarambil, S.; Colice, G. Tezepelumab in Adults and Adolescents with Severe, Uncontrolled Asthma. *N. Engl. J. Med.* **2021**, *384*, 1800−1809.
(27) Hoy, S. M. Tezepelumab: First Approval. *Drugs* **2022**, *82*, 461−468.
(28) Gauvreau, G. M.; Hohlfeld, J. M.; FitzGerald, J. M.; Boulet, L. P.; Cockcroft, D. W.; Davis, B. E.; Korn, S.; Kornmann, O.; Leigh, R.;

https://doi.org/10.1021/acs.jmedchem.3c02163
J. Med. Chem. XXXX, XXX, XXX−XXX

Mayers, I.; Watz, H.; Grant, S. S.; Jain, M.; Cabanski, M.; Pertel, P. E.; Jones, I.; Lecot, J. R.; Cao, H.; O'Byrne, P. M. Inhaled Anti-Tslp Antibody Fragment, Ecleralimab, Blocks Responses to Allergen in Mild Asthma. *Eur. Respir. J.* **2023**, *61*, No. 2201193.
(29) O'Byrne, P. M.; Panettieri, R. A.; Taube, C.; Brindicci, C.; Fleming, M.; Altman, P. Development of an Inhaled Anti-Tslp Therapy for Asthma. *Pulm. Pharmacol. Ther.* **2023**, *78*, No. 102184.
(30) Park, B. B.; Choi, J. W.; Park, D.; Choi, D.; Paek, J.; Kim, H. J.; Son, S.-Y.; Mushtaq, A. U.; Shin, H.; Kim, S. H.; Zhou, Y.; Lim, T.; Park, J. Y.; Baek, J.-Y.; Kim, K.; Kwon, H.; Son, S.-H.; Chung, K. Y.; Jeong, H.-J.; Kim, H.-M.; Jung, Y. W.; Lee, K.; Lee, K. Y.; Byun, Y.; Jeon, Y. H. Structure-Activity Relationships of Baicalein and Its Analogs as Novel Tslp Inhibitors. *Sci. Rep.* **2019**, *9*, No. 8762.
(31) Park, S.; Park, Y.; Son, S.-H.; Lee, K.; Jung, Y. W.; Lee, K. Y.; Jeon, Y. H.; Byun, Y. Synthesis and Biological Evaluation of Peptide-Derived Tslp Inhibitors. *Bioorg. Med. Chem. Lett.* **2017**, *27*, 4710−4713.
(32) Van Rompaey, D.; Verstraete, K.; Peelman, F.; Savvides, S. N.; Augustyns, K.; Van Der Veken, P.; De Winter, H. Virtual Screening for Inhibitors of the Human Tslp:Tslpr Interaction. *Sci. Rep.* **2017**, *7*, No. 17211.
(33) Heinis, C.; Rutherford, T.; Freund, S.; Winter, G. Phage-Encoded Combinatorial Chemical Libraries Based on Bicyclic Peptides. *Nat. Chem. Biol.* **2009**, *5*, 502−507.
(34) Teufel, D. P.; Bennett, G.; Harrison, H.; van Rietschoten, K.; Pavan, S.; Stace, C.; Le Floch, F.; Van Bergen, T.; Vermassen, E.; Barbeaux, P.; Hu, T.-T.; Feyen, J. H. M.; Vanhove, M. Stable and Long-Lasting, Novel Bicyclic Peptide Plasma Kallikrein Inhibitors for the Treatment of Diabetic Macular Edema. *J. Med. Chem.* **2018**, *61*, 2823−2836.
(35) Baeriswyl, V.; Calzavarini, S.; Chen, S.; Zorzi, A.; Bologna, L.; Angelillo-Scherrer, A.; Heinis, C. A Synthetic Factor Xiia Inhibitor Blocks Selectively Intrinsic Coagulation Initiation. *ACS Chem. Biol.* **2015**, *10*, 1861−1870.
(36) Chalmers, M. J.; Busby, S. A.; Pascal, B. D.; West, G. M.; Griffin, P. R. Differential Hydrogen/Deuterium Exchange Mass Spectrometry Analysis of Protein−Ligand Interactions. *Expert Rev. Proteomics* **2011**, *8*, 43−59.
(37) James, E. I.; Murphree, T. A.; Vorauer, C.; Engen, J. R.; Guttman, M. Advances in Hydrogen/Deuterium Exchange Mass Spectrometry and the Pursuit of Challenging Biological Systems. *Chem. Rev.* **2022**, *122*, 7562−7623.
(38) Konermann, L.; Pan, J.; Liu, Y.-H. Hydrogen Exchange Mass Spectrometry for Studying Protein Structure and Dynamics. *Chem. Soc. Rev.* **2011**, *40*, 1224−1234.
(39) Cromm, P. M.; Schaubach, S.; Spiegel, J.; Furstner, A.; Grossmann, T. N.; Waldmann, H. Orthogonal Ring-Closing Alkyne and Olefin Metathesis for the Synthesis of Small Gtpase-Targeting Bicyclic Peptides. *Nat. Commun.* **2016**, *7*, No. 11300.
(40) Saxton, R. A.; Glassman, C. R.; Garcia, K. C. Emerging Principles of Cytokine Pharmacology and Therapeutics. *Nat. Rev. Drug Discovery* **2023**, *22*, 21−37.
(41) Matthews, A. A.; Ee, P. L. R.; Ge, R. Developing Inhaled Protein Therapeutics for Lung Diseases. *Mol. Biomed.* **2020**, *1*, No. 11.
(42) Fellner, R. C.; Terryah, S. T.; Tarran, R. Inhaled Protein/Peptide-Based Therapies for Respiratory Disease. *Mol. Cell. Pediatr.* **2016**, *3*, No. 16.
(43) Wesche, F.; De Maria, L.; Leek, T.; Narjes, F.; Bird, J.; Su, W.; Czechtizky, W. Automated High-Throughput in Vitro Assays to Identify Metabolic Hotspots and Protease Stability of Structurally Diverse, Pharmacologically Active Peptides for Inhalation. *J. Pharm. Biomed. Anal.* **2022**, *211*, No. 114518.
(44) Wesche, F.; De Maria, L.; Leek, T.; Narjes, F.; Bird, J.; Su, W.; Czechtizky, W. Analyzing Proteolytic Stability and Metabolic Hotspots of Therapeutic Peptides in Two Rodent Pulmonary Fluids. *J. Pharm. Biomed. Anal.* **2023**, *224*, No. 115156.
(45) Klein, T.; Vajpai, N.; Phillips, J. J.; Davies, G.; Holdgate, G. A.; Phillips, C.; Tucker, J. A.; Norman, R. A.; Scott, A. D.; Higazi, D. R.; Lowe, D.; Thompson, G. S.; Breeze, A. L. Structural and Dynamic Insights into the Energetics of Activation Loop Rearrangement in Fgfr1 Kinase. *Nat. Commun.* **2015**, *6*, No. 7877.
(46) Vagin, A.; Teplyakov, A. Molecular Replacement with Molrep. *Acta Crystallogr., Sect. D: Biol. Crystallogr.* **2010**, *66*, 22−25.
(47) Murshudov, G. N.; Vagin, A. A.; Dodson, E. J. Refinement of Macromolecular Structures by the Maximum-Likelihood Method. *Acta Crystallogr., Sect. D: Biol. Crystallogr.* **1997**, *53*, 240−255.
(48) Emsley, P.; Lohkamp, B.; Scott, W. G.; Cowtan, K. Features and Development of Coot. *Acta Crystallogr., Sect. D: Biol. Crystallogr.* **2010**, *66*, 486−501.
(49) Wodak, S. J.; Janin, J. Structural Basis of Macromolecular Recognition. *Adv. Protein Chem.* **2002**, *61*, 9−73.

https://doi.org/10.1021/acs.jmedchem.3c02163
J. Med. Chem. XXXX, XXX, XXX−XXX